NeuroImage 245 (2021) 118650

Contents lists available at ScienceDirect

NeuroImage

journal homepage: www.elsevier.com/locate/neuroimage

Neural basis of distractor resistance during visual working memory maintenance

Petra Hermann[†], Béla Weiss[†], Balázs Knakker, Petra Madurka, Annamária Manga, Ádám Nárai, Zoltán Vidnyánszky[*]

Brain Imaging Centre, Research Centre for Natural Sciences, Budapest H-1117, Hungary

ARTICLE INFO

Keywords:
Working memory
Attention
Distractor resistance
EEG
fMRI

ABSTRACT

Visual working memory representations must be protected from the intervening irrelevant visual input. While it is well known that interference resistance is most challenging when distractors match the prioritised mnemonic information, its neural mechanisms remain poorly understood. Here, we identify two top-down attentional control processes that have opposing effects on distractor resistance. We reveal an early selection negativity in the EEG responses to matching as compared to non-matching distractors, the magnitude of which is negatively associated with behavioural distractor resistance. Additionally, matching distractors lead to reduced post-stimulus alpha power as well as increased fMRI responses in the object-selective visual cortical areas and the inferior frontal gyrus. However, the congruency effect found on the post-stimulus periodic alpha power and the inferior frontal gyrus fMRI responses show a positive association with distractor resistance. These findings suggest that distractor interference is enhanced by proactive memory content-guided selection processes and diminished by reactive allocation of top-down attentional resources to protect memorandum representations within visual cortical areas retaining the most selective mnemonic code.

1. Introduction

Protection of visual working memory (WM) representations from the interference posed by the incoming task-irrelevant visual input is critically important for efficient WM under real-life conditions. Distractor interference resistance has shown to be particularly challenging when irrelevant distractors match the WM content and there is a substantial overlap in their neural representations (Clapp et al., 2010; Dolcos et al., 2007; Sreenivasan and Jha, 2007; Yoon et al., 2006). In spite of the extensive previous research effort, the neural processes underlying the mitigation of the interference caused by external delay distractors are poorly understood. Traditionally, it was assumed that distractor resistance might be accomplished by the same top-down attentional selection processes that are active during visual perception (Awh and Jonides, 2001; Chun et al., 2011; Clapp et al., 2010; Desimone and Duncan, 1995; Dolcos et al., 2007; Gazzaley, 2011; Gazzaley and Nobre, 2012; Kiyonaga and Egner, 2013; Sreenivasan and Jha, 2007; Yoon et al., 2006). According to the biased competition model of attentional control (Desimone and Duncan, 1995), allocation of feedback attentional resources is implemented via attentional templates maintained in WM. The WM-content-based attentional templates are facilitative (Desimone and Duncan, 1995; Egner and Hirsch, 2005; Nelissen et al., 2013) and lead to enhanced visual cortical processing of task-relevant information, which in turn will bias the inherent competitive interactions between the processing of concurrent visual inputs, resulting in diminished representation of task-irrelevant, distracting information. In line with this, research using the retro-cueing paradigm (Griffin and Nobre, 2003; Landman et al., 2003) provided evidence that attentional templates can be directed towards specific visual feature and object representations stored in WM resulting in increased WM performance (for review see Souza and Oberauer, 2016). It has also been shown that attentional selection of mnemonic information leads to enhanced WM delay neural activity within the visual cortical areas involved in the processing of the selected features during perception (Gazzaley, 2011; Lepsien and Nobre, 2007; Myers et al., 2017; Nelissen et al., 2013; Sligte et al., 2009) and that the source of this top-down control signal lies in the ventrolateral prefrontal cortex (Lepsien and Nobre, 2007; Myers et al., 2017; Nee and Jonides, 2009).

However, whether and how top-down attentional processes of prioritisation of WM representations might contribute to interference resistance in the case of external distractors, remain unresolved questions. Previous research failed to provide support for the existence of

* Corresponding author.
E-mail address: vidnyanszky.zoltan@ttk.hu (Z. Vidnyánszky).
† These authors contributed equally to the presented work.

https://doi.org/10.1016/j.neuroimage.2021.118650.
Received 7 July 2021; Received in revised form 10 September 2021; Accepted 11 October 2021
Available online 20 October 2021.

proactive negative attentional templates inhibiting the visual cortical processing of delay distractors (for recent reviews see Chelazzi et al., 2019; de Vries et al., 2020; Noonan et al., 2018), which is in agreement with the facilitative nature of attentional templates (Desimone and Duncan, 1995; Egner and Hirsch, 2005; Nelissen et al., 2013). In line with this, recent human neuroimaging results (Rademaker et al., 2019) showed that feedback-based WM-content-related and bottom-up distractor-related information are simultaneously represented in the visual cortex. Furthermore, several previous studies found that mnemonic content automatically guides attention to a matching item in an unrelated visual search task performed during the WM maintenance period (Olivers et al., 2011, 2006; Soto et al., 2008) as well as enhanced visual cortical functional magnetic resonance imaging (fMRI) responses for delay distractors when they match the WM content as compared to when they differ from it (Dolcos et al., 2007; Gayet et al., 2017; Jha et al., 2004; Yoon et al., 2006). Taken together, these findings raise the hypothesis that processing of distractor objects matching the WM content will be affected by two different top-down attentional mechanisms: 1. WM-content-guided proactive attentional selection processes that will automatically enhance early distractor processing and diminish distractor resistance; 2. Reactive allocation of top-down attentional resources to protect WM content within visual cortical areas retaining the most selective memorandum representation and thus foster distractor resistance.

We addressed this hypothesis by investigating the neural responses to face distractors presented during the WM maintenance of unfamiliar face identity or grating orientation information. In congruent and incongruent conditions the face distractors were matching to or differing from the memorandum category, respectively, allowing us to test congruency effects. Sample stimuli involved superimposed face and grating object images. Retro-cueing (Griffin and Nobre, 2003; Landman et al., 2003; Souza and Oberauer, 2016) was used to indicate whether face identity or grating orientation information had to be compared with the probe stimulus on a given trial. Because of this, encoding of the sample stimuli did not differ between the face identity and grating orientation WM conditions, ensuring that the modulation of delay distractor processing originates from top-down attentional control processes. All stimuli were displayed at the centre of fixation to avoid spatial attention-based selection.

We expected to find WM-content-guided attentional modulation of distractor-evoked electroencephalogram (EEG) responses depending on distractor congruency, as reflected in the presence of selection negativity (SN) – a well-characterised marker of proactive attentional selection of nonspatial visual features and shapes (Hillyard and Anllo-Vento, 1998; Keil and Müller, 2010; Kenemans et al., 1993; Previc and Harter, 1982; Smid et al., 1999) – in the case of congruent as compared to incongruent distractors. To provide support for the involvement of reactive top-down attentional selection processes in the protection of task-relevant memorandum representations, we measured congruency effects on post-stimulus EEG alpha power reflecting allocation of feedback attentional resources to visual information processing within the visual cortex (Grill-Spector et al., 2017; Stigliani et al., 2019; Weiner et al., 2010) as well as on distractor-related visual cortical and prefrontal fMRI responses. Our fMRI analysis was focused on the face-selective visual cortical areas (Duchaine and Yovel, 2015; Freiwald et al., 2016; Grill-Spector et al., 2017) – the occipital face area (OFA) and the two subregions of the fusiform face area (FFA), namely the pFus-faces/FFA-1 and the mFus-faces/FFA-2 – as well as on the ventrolateral prefrontal cortex (vlPFC), in particular the pars triangularis of the inferior frontal gyrus (PT-IFG), considered to be the source of top-down attentional selection between WM memorandum representations (Dolcos et al., 2007; Jha et al., 2004; Lepsien and Nobre, 2007; Nee et al., 2013; Nee and Jonides, 2009). Importantly, we also predicted that the participants' behavioural distractor resistance measured on WM performance would be negatively associated with SN and positively associated with the strength of post-stimulus alpha power and fMRI congruency effects driven by the proactive and reactive attentional selection processes, respectively. The results obtained in the present study provide experimental support for our predictions by revealing: 1. SN in congruent as compared to incongruent face-distractor-related EEG responses, the magnitude of which showing a negative association with the participants' behavioural distractor resistance; 2. Significant face-distractor-related congruency effects on the post-stimulus alpha power as well as on the mFus-faces/FFA-2 and the PT-IFG fMRI responses. Importantly, the strength of congruency effects on both post-stimulus periodic alpha power and PT-IFG activation show a positive correlation with the participants' behavioural distractor resistance.

2. Material and methods

2.1. Participants

The study included the same 36 participants in the EEG and fMRI experiments. We planned to conduct the fMRI experiment before the EEG experiment due to the relatively high dropout rate common in fMRI studies. In the case of 25 participants the fMRI experiment was performed first, while in the case of 11 participants the fMRI experiment was performed after the EEG experiment because of delays in MRI scanner availability. We excluded 2 participants from further analysis due to poor task performance and one participant with incomplete data acquisition resulting in a sample size of N = 33 (age range: 18–26 years; age mean ± standard deviation (SD): 21.4 ± 1.9 years; 20 female). Each participant was right-handed and had normal or corrected-to-normal vision including intact colour-vision, with no reported history of neurological or psychiatric diseases. All participants provided written, informed consent before participation and were financially compensated for their time. The research was approved by the National Institute of Pharmacy and Nutrition (file number: OGYÉI/70,184/2017). Participants' data obtained separately in the orientation delayed-estimation task (see later) was reported in our previous paper (Manga et al., 2020) as part of a larger sample.

2.2. EEG experiment

2.2.1. Stimuli and procedure

During the EEG experiment, participants performed a retro-cued Sternberg WM task with faces and simple grating patterns, with distracting face stimuli appearing in the delay period (Fig. 1). Experimental sessions started with a short verbal briefing followed by 1–4 training blocks, each consisting of 32 distractor-free trials and lasting 5–10 min. The training phase was concluded when the participant performed at least at 70%, which was checked after each block. The time needed for this varied across participants, partly due to prior experience with similar tasks. The EEG cap was applied at this point, and the main phase of the experiment was started. The EEG recording lasted approximately 90–120 min, an entire experimental session took 3–3.5 h. Participants were seated 56 cm from an LCD display (1920 × 1200 pixels resolution, 55 cm wide, 60 Hz refresh rate), with their head positioned using the chin rest of the eye tracker. Participants' fixation was monitored online and their gaze position was recorded (SMI Hi-Speed and SMI iView X 2.4 software, Sensomotoric Instruments, Teltow, Germany). A blue fixation disc (d = 0.4°) was always present at the centre of the screen, the background was mid-grey. All trials started with two sample stimuli, each lasting 800 ms, with an interstimulus interval (ISI) of 200 ms in between. Sample stimuli were compound face-grating stimuli; linearly blended (with equal weights) contrast and luminance-equated images of faces and simple sinusoid grating patterns (see details below). The second sample was followed by an 800 ms blank period, after which a symbolic retro-cue appeared for 500 ms, which indicated whether the identity of the two faces (face identity WM trials) or the orientation of the two gratings (grating orientation WM trials) were to be probed at the end of the trial. The face identity WM and grating orientation WM

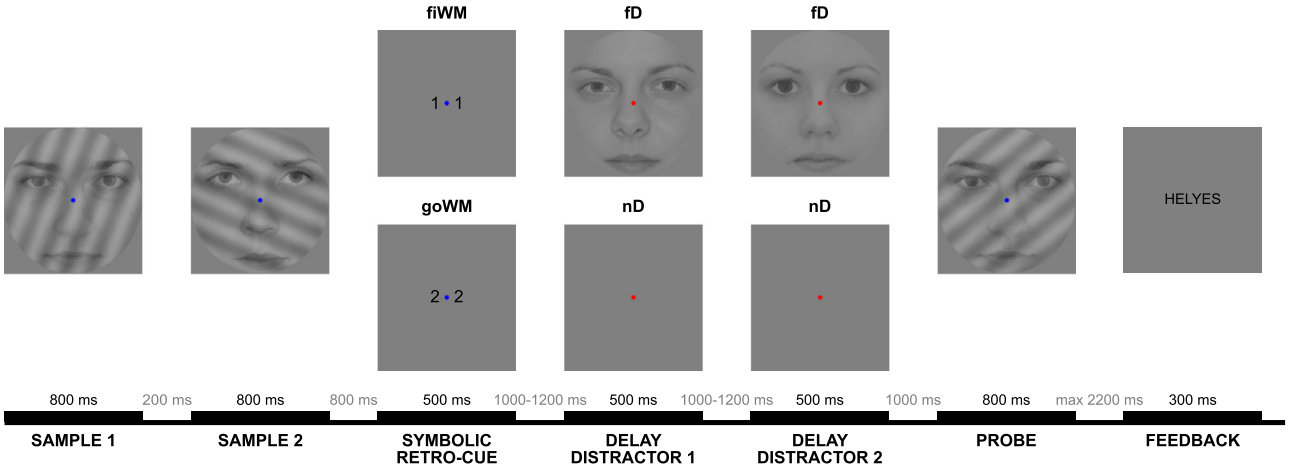

Fig. 1. Schematic illustration of one trial in the EEG experiment. Participants performed a retro-cued Sternberg working memory task with faces and simple grating patterns, without distractor (nD) or with face distractor (fD) stimuli appearing in the delay period. A symbolic retro-cue indicated whether the identity of the two faces (face identity working memory, fiWM) or the orientation of the two gratings (grating orientation working memory, goWM) were to be probed at the end of the trial.

trials occurred with 50% probability, in randomised order. Retro-cues were numbers (1 and 2, mapping to faces and gratings counterbalanced across participants) displayed at both sides of the fixation disc (printed in 20 pt Arial at the centre of the screen, separated by a space for the fixation disc). Evidently, participants did not know in advance which category would be relevant when they saw the sample stimuli, and they were explicitly instructed to try to memorise both gratings and faces – achieving this was of primary importance in the training phase. After a delay jittered between 1000 and 1200 ms, the time window of the distractor lasted for 500 ms, during which the fixation disc was red, and a distractor could appear (see below). This was followed by a second distractor with the same timing (1000–1200 ms ISI from the first distractor offset to the second distractor onset, 500 ms display time).

After an additional delay of 1000 ms, the probe was displayed for 800 ms. The probe was also a composite image prepared using the same method as the sample stimuli. The irrelevant image component in the probe was always different from all previous stimuli in the current trial. The relevant image component (as indicated by the retro-cue) was either also different from all others of the trial ('new' trials), or it was one of the probe stimuli from the current trial reoccurring ('old' trials). The probe types came in randomised order, with equal numbers within each condition (new – 50%; old, first sample – 25%; old, second sample – 25%). Participants had to indicate whether they saw an old or a new probe, with pressing the keys 7 and 8 (mapping counterbalanced across participants) on a numeric keyboard. Response hand was randomised and counterbalanced across participants. The response time window started at probe onset and was terminated when a response was given and the probe was offscreen, or after a 3-sec timeout. After the response window, participants received feedback in form of text at the centre of the screen saying either 'correct' or 'wrong' in Hungarian, displayed for 300 ms in 20 pt Arial. If the response window timed out, the text 'faster!' appeared as a feedback. Participants were told at the beginning of the experiment that this prompt was not intended to instruct them to favour speed at the expense of accuracy, but is rather important during the training phase to help them catch the general pace of the experiment. After an ISI of 1000 or 1200 ms (occurring randomly), the next trial started.

With respect to the delay distractor, there were 2 trial types. During no distractor trials, the fixation disc turned red for 500 ms and no face stimulus was presented. On face distractor trials, two face images were drawn from the stimulus pool that were different from all other stimuli in the current trial. Each distractor was blended with the background colour with 50–50% weights to match the contrast of one component in the compound sample stimulus.

A temporal succession of two face distractors was presented in the delay periods throughout 6 runs of 48 trials each, and no distractor in 2 runs (always the 3rd and the 6th run). There were self-paced rest periods between experimental runs, and also a smaller break at the half of each run.

All stimuli subtended 3° of visual angle both horizontally and vertically. Face images (117 male, 120 female) were front-view grayscale photographs cropped with a circular masque with a diameter of 3° of visual angle to eliminate external facial features and equated for contrast and luminance. Within one trial, only male or only female faces were used; male and female trials came in random order, counterbalanced across conditions. Grating images were sinusoid gratings in a 3° of visual angle circular aperture having a spatial frequency of 2 cycles per degree, with luminance and contrast matched to the face stimuli. There were six grating directions, spanning non-cardinal directions between horizontal and vertical equally (22.5°, 45°, 67.5°, 112.5°, 135°, 157.5°). Within one trial, no grating or face stimulus was repeated except for the case when they were displayed as an 'old' probe. In addition, to minimize direct interference from face identities repeating in neighbouring trials, face stimuli were pseudo-randomly drawn with replacement from the male or the female image set so that there were at least 60 draws between two occurrences of the same face.

Presentation of stimuli, control of the experimental procedure and collection of participants' responses were performed using custom-written scripts and the Psychophysics Toolbox (Brainard, 1997; Pelli, 1997) 3.0.9 under MATLAB R2008a (The MathWorks Inc., Natick, MA, USA).

2.2.2. *Electrophysiological recording and analysis*

For the recording of EEG data a 96-channel ActiCap system was used with 3 BrainAmp MR plus amplifiers and BrainVision Recorder 1.2 software (Brain Products GmbH, Munich, Germany). The electrodes were fitted on an elastic cap (EasyCap GmbH, Herrsching, Germany). Impedance was lowered and kept below 5 kΩ throughout the experiments. Scalp electrodes were positioned according to 10/5 standard, and an additional vertical electrooculogram ($vEOG_L$) electrode was positioned below the right eye. All electrodes were referenced to the right mastoid (TP10), and the ground electrode was located at position FPz. The EEG signal was sampled at 2500 Hz.

All preprocessing was performed in MATLAB R2015a (The MathWorks Inc., Natick, MA, USA) using EEGLAB (Delorme and Makeig, 2004) 13.4.4.b, ERPLAB (Lopez-Calderon and Luck, 2014) 5.0 and custom-written scripts. First, data was downsampled to 500 Hz

(pop_resample() from EEGLAB). Bandpass filtering was performed using the pop_basicfilter() function from the ERPLAB toolbox. For blink detection, event-related potential (ERP) analysis and time-frequency analysis, data were filtered with fourth-order Butterworth zero-phase filters with half-amplitude cutoffs (half-power cutoff shown in parentheses) at 0.1 Hz (0.1 Hz) for high-pass and 37.5 Hz (30.3 Hz) for low-pass. For further artefact detection, the low-pass half-amplitude cutoff was 84.4 Hz (70 Hz), while high-pass was identical. For Independent Component Analysis (ICA), the high-pass cutoff was set to 0.4 Hz (0.5 Hz), as ICA is known to be overly sensitive to low-frequency drifts in the signal. A notch filter at 50 Hz was applied in each case using a Q-factor of 45 (bandwidth at −1 dB: 1.11 Hz) using MATLAB functions iirnotch(), dfilt.df2() and filtfilt().

Segments time-locked to the first sample stimulus (from −600 ms to 800 ms relative to onset), the second sample stimulus (−200 to 1000 ms), the retro-cue (−600 to 1500 ms), the distractors (−600 to 1500 ms) and the probe (−600 to 1000 ms) were created for artefact rejection purposes. Putative eye blinks were detected using a semi-automatic thresholding procedure based on the bipolar vertical EOG calculated as FP2-vEOG$_L$. The aim of the next step was to identify artefacts that are unsuitable to be removed in the subsequent cleaning step that is based on ICA. First, automatic artefact detection was performed using EEGLAB functions, which was then overruled by careful trial-by-trial visual inspection. Based on the first artefact rejection step, time points deemed suitable for ICA were selected (without segment overlap, i.e. avoiding sampling the same data point more than once) from the continuous dataset. This data was filtered with the 0.4 Hz cutoff and subjected to ICA decomposition with the extended Infomax algorithm (Bell and Sejnowski, 1995; Onton et al., 2006) with a maximum of 1024 iterations and a stopping threshold of 10^{-7}. ICA was preceded by dimension reduction to 64 components using Principal Component Analysis. Using the weights from this decomposition, the dataset with the widest filters (0.1 to 84.4 Hz) was projected to component space, and components with well-isolated artefactual activity and without substantial signal content were discarded (Chaumon et al., 2015; Delorme et al., 2007) based on topographies and activations (averages, spectra and single-trial time courses). Not discarding any signal content was prioritised over potentially removing more artefacts, i.e. ambiguous components were kept, and the corresponding problematic trials were discarded in the next step, when the data projected to the "clean" subspace were visually inspected for artefacts once again.

Statistical evaluation of distractor congruency effects on EEG activity and post-stimulus alpha power was based on average-referenced EEG segments time-locked to the onset of first distractor stimuli. Only trials with artefact-free distractor-related segments were considered, the number (mean ± SD, minimum, maximum) of clean trials per condition was as follows: face identity WM – face distractor (82 ± 13, 50, 107), grating orientation WM – face distractor (93 ± 16, 62, 126). In the case of EEG activity analysis, baseline correction was carried out at single-trial level by subtracting the average EEG activity in the [−600, 0] ms pre-stimulus baseline interval from all samples. Subject-level EEG averages were generated by taking the arithmetic mean of baseline-corrected trials for all conditions separately.

The time course of post-stimulus alpha power was characterized by baseline-corrected EEG power of the 8–13 Hz alpha frequency band. Continuous wavelet transformation (MATLAB cwt() function with 'cmor1–1′ input argument for complex Morlet wavelets with Fb = 1 bandwidth parameter and Fc = 1 wavelet centre frequency) was applied on clean EEG segments to obtain the power (squared amplitude of complex wavelet coefficients) of EEG oscillatory activity from 8 Hz to 13 Hz with 1 Hz resolution for all sample points. Baseline correction was performed at single-trial level by dividing all power samples by the average power in the [−400, −100] ms baseline pre-stimulus time interval. The [−600, −400] ms and the [−100, 0] ms intervals of EEG segments were excluded from calculation of the average baseline power to prevent the inclusion of wavelet calculation edge-effects and potential smearing of early evoked alpha power into the baseline interval, respectively. Subject-level averages of post-stimulus alpha power time course were calculated by taking the arithmetic mean of baseline-corrected trials ($P_{\alpha bc}$) for all conditions separately. Base-10 logarithm of subject-level averages was taken and multiplied by 10 ($10\log_{10}P_{\alpha bc}$) to obtain the power values in decibels (dB). Finally, averaging over the frequency dimension was carried out in the 8–13 Hz alpha frequency band.

Distractor congruency effects on EEG activity and post-stimulus alpha power time course were assessed by mass univariate analysis of subject-level averages considering all EEG electrode × time sample pairs in the whole [0, 1500] ms post-stimulus time interval after the onset of distractors. No false distractor congruency effects were found that could be generated at the end of the segments by the edge-effects of wavelet transformation used for estimation of post-stimulus alpha power time course. Central tendency of EEG activity and post-stimulus alpha power time course was compared between congruent and incongruent face distractor conditions (face identity WM – face distractor vs grating orientation WM – face distractor) using paired-samples t-tests ($P < 0.05$). Multiple comparisons correction was carried out by applying the cluster-based permutation testing framework (Maris and Oostenveld, 2007; Nichols and Holmes, 2002) implemented in the FieldTrip toolbox (Oostenveld et al., 2010) (revision 1d5ddcf). The number of randomisations was 9999. Spatial neighbourhood was calculated using the ft_prepare_neighbours() FieldTrip function with 5 cm neighbour distance, and the required minimum number of neighbours with significant effect was 2 for generation of clusters. Clusters were characterised by their 'maxsum' statistic, and positive and negative clusters were assessed together by using a 0.025 cluster significance level. To present the EEG results in the same form as the fMRI results, the original cluster P_{clust} values were multiplied by 2 ($P_c = 2 \times P_{clust}$), and accordingly, clusters with corrected $P_c < 0.05$ values were considered significant. P_c values of positive and negative clusters were denoted by P_{cp} and P_{cn}, respectively. If a particular test resulted in multiple significant clusters of same polarity, clusters were sorted in an ascending order according to their P_c values and an additional index was added to their subscript (e.g. P_{cn2} would denote the second most significant negative cluster). Wavelet transformation and statistical analysis were carried out in MATLAB 2013b (The MathWorks Inc., Natick, MA, USA) using custom-written scripts.

Using a recently published method (Donoghue et al., 2020) we further investigated face distractor congruency effects on post-stimulus alpha power while controlling for the effects of aperiodic components. For this analysis we used the time range of significant congruency effect on post-stimulus alpha power time course (from 350 to 950 ms relative to distractor onset) and an equal length baseline segment from −600 to 0 ms relative to distractor onset. Power spectral density estimation and spectral parametrization was applied on trial-level. Power spectral density was estimated using the periodogram() function from the scipy (1.6.2) package (Virtanen et al., 2020) with 2000 point FFT length and a Hann window. Spectral parametrization was performed using the FOOOF (1.0.0) package (Donoghue et al., 2020) with the following parameters: freq_range = [3, 25], peak_width_limits = [1, 6], max_n_peaks = 6, min_peak_height = 0.05, peak_threshold = 1.5 and aperiodic_mode = 'fixed'. Power values were converted to dB by taking their base-10 logarithm multiplied by 10. We calculated alpha power measures by taking the 8–13 Hz band average for both the evoked and baseline segments of each trial. Total alpha power was derived from the total power spectrum, aperiodic alpha power was derived from the fitted aperiodic component, and periodic alpha power was derived from the flattened spectrum (total power spectrum − aperiodic power spectrum). Finally, baseline alpha power measures were subtracted from the corresponding evoked alpha power measures. Post-stimulus alpha power was averaged across trials within both conditions (face identity WM – face distractor and grating orientation WM – face distractor) and two-tailed paired-samples t-tests ($P_c < 0.05$) were performed between the two conditions with 1D spatial clustering, using the permutation_cluster_1samp_test()

function from the mne (0.22.0) package (Gramfort et al., 2013) and the same neighbourhood matrix as in the time course analysis.

2.3. fMRI experiment

2.3.1. Stimuli and procedure

The participants of the EEG experiment performed a retro-cued Sternberg WM task with the same stimuli and experimental design used in the EEG experiment (for details, see Section 2.2.1), but only with the first distractor time window in the delay period, in which either a face distractor or a grating distractor stimulus was presented intermixed in random order (the no distractor condition was not used) and with timing optimised for fMRI. To be able to separately model the blood-oxygen-level-dependant (BOLD) response to distractor stimulus we used temporally jittered ISI of 3500, 4500, 5500, and 6500 ms, which separated the 500-ms-long distractor from the 500-ms-long retro-cue and probe stimuli so that the delay period (i.e. the time interval between retro-cue offset and probe onset) had a fixed duration of 10,500 ms. The within-trial ISI levels were randomised and counterbalanced across conditions. The trials were separated by jittered ISI (between probe offset and next trial sample onset) with 4 levels linearly spaced between 7100 and 10,100 ms. The 2500 ms response time window started at probe onset, after which participants did not receive feedback regarding their response. 900 ms before each trial the fixation dot colour changed from blue to green for 200 ms cueing the beginning of the next trial. The between-trial ISI levels were randomised across the 32 trials in a run and a ~30 s baseline epoch with a fixation dot was placed before the 1st, 12th and 23rd trial.

Stimuli were displayed centrally, subtending 3 × 3° (rescaled by either + or − 30% in the case of distractor stimuli, randomised and counterbalanced across conditions), on a uniform grey background on an MRI-compatible LCD screen (32′ NNL LCD Monitor, NordicNeuroLab, Bergen, Norway; 1920 × 1080 pixels resolution; 60 Hz refresh rate) placed at 142 cm from the observer and were viewed via a mirror attached to the top of the head coil. Head motion was minimized using foam padding. Participants' responses were collected using two buttons of the ResponseGrip (NordicNeuroLab, Bergen, Norway). Button mapping and response hand was randomised and counterbalanced across participants.

Presentation of stimuli, control of the experimental procedure and collection of participants' responses were performed using custom-written scripts and the Psychophysics Toolbox (Brainard, 1997; Pelli, 1997) 3.0.14 under MATLAB R2015a (The MathWorks Inc., Natick, MA, USA).

The fMRI experiment consisted of two fMRI sessions including 3 × ~14-min-long WM runs each, yielding 192 trials in 6 runs altogether. In order to define face-selective visual cortical areas, a separate ~8.5-min-long functional localiser run was also conducted after the experimental runs in the second fMRI session (6 × 12 s epochs of face, house, and human body images, interleaved with 12, 15, or 18 s of rest periods with only the fixation dot present; 1 Hz stimulus presentation rate; 500 ms exposition time; 500 ms ISI).

2.3.2. fMRI data acquisition and analysis

2.3.2.1. Data acquisition. Data were acquired on a Siemens Magnetom Prisma 3T MRI scanner (Siemens Healthcare GmbH, Erlangen, Germany) at the Brain Imaging Centre, Research Centre for Natural Sciences. All head elements of the standard Siemens 64-channel head-neck receiver coil were applied. For functional measurements a blipped-controlled aliasing in parallel imaging (CAIPI) simultaneous multi-slice gradient-echo-EPI sequence (Setsompop et al., 2012) was used with 6-fold slice acceleration. Full brain coverage was obtained with an isotropic 2 mm spatial resolution (208 × 208 mm field-of-view (FOV); anterior-to-posterior phase encoding direction; 104 × 104 in-plane matrix size; 54 slices; 25% slice gap) and a repetition time (TR) of 710 ms, without in-plane parallel imaging. A partial Fourier factor of 7/8 was used to achieve an echo time (TE) of 30 ms. Flip angle (FA) was 59°. Image reconstruction was performed using the Slice-GRAPPA algorithm (Setsompop et al., 2012) with LeakBlock kernel (Cauley et al., 2014). T1-weighted 3D MPRAGE anatomical imaging was performed using 2-fold in-plane GRAPPA acceleration with isotropic 1 mm spatial resolution (TR/TE/FA = 2300 ms/3 ms/9°; FOV = 256 × 256 mm).

2.3.2.2. Data preprocessing and statistical analyses. The functional images were spatially realigned using SPM's two pass procedure. All realigned functional images were coregistered with the 3D anatomical image, which was then segmented and normalised to the Montreal Neurological Institute (MNI)−152 space ($2 \times 2 \times 2$ mm^3) using the unified segmentation-normalisation tool of SPM12. To spatially normalise functional images to MNI-152 space, we applied the deformation field parameters that were obtained during the normalisation of the 3D anatomical image. After the normalisation procedure, functional images were spatially smoothed with a 5-mm full-width at half-maximum isotropic Gaussian kernel.

For first-level statistical analysis of fMRI data we used a standard voxel-wise General Linear Model (GLM) implemented in SPM12, with regressors as boxcar functions convolved with SPM's canonical hemodynamic response function and applied a temporal high-pass filter with a cutoff frequency of 1/128 Hz. The following regressors representing the different task conditions were used: face identity WM and grating orientation WM in the sample/retro-cue time window; face identity WM – face distractor, grating orientation WM – face distractor, face identity WM – grating distractor and grating orientation WM – grating distractor in the distractor time window; face identity WM and grating orientation WM in the probe time window. Movement-related variance was accounted for by including the estimated movement parameters resulting from the motion correction procedure as nuisance covariates in the design matrix. Temporal autocorrelations were modelled with SPM's FAST model. The first-level contrast images derived from parameter estimates (β values) of the defined regressors served as input for the second-level whole-brain random-effects statistical analyses (one-sample t-tests). For the localiser run the same GLM procedure was applied with face, house and body regressors, where face vs house and body vs house contrast images served as input for the first-level fixed-effects statistical analyses (one-sample t-tests). Significance testing of first- and second-level t-maps was performed using two-tailed voxel-level False Discovery Rate (FDR) at q = 0.05 as correction for multiple comparisons.

For region of interest (ROI)-based analyses, percent signal change (PSC) was computed using the method suggested by Pernet (2014) and Poldrack et al. (2011). Mean PSCs were extracted from a sphere with 5 mm radius around the peak voxel of each participant's individually defined ROI and entered into a second-level three-way repeated-measures analysis of variance (ANOVA) with WM content (face identity WM vs grating orientation WM), Distractor category (face distractor vs grating distractor), and ROI as within-subject factors. Significance testing was performed using a permutation-based approach with 9999 iterations. Interaction and main effect P values were calculated by comparing the F-statistic of intact data to its null distribution computed by randomly shuffling condition labels within each subject. Simple effects testing was performed using paired-samples t-tests, and two-tailed P values corrected for multiple comparisons were derived using the permutation-based maximum statistic method (Nichols and Holmes, 2002). We generated the null distributions of maximum t values by randomly shuffling condition labels per subject and taking the maximum of absolute t values across the comparisons within one factor on each iteration. We used the resulting null distribution to determine corrected P values, which was provided as $P_{c,N}$ with N marking the number of comparisons corrected for when N > 1. Note that due to performing permutation testing with 9999 iterations, the resolution of our P values has a lower limit of P = 0.0001.

Preprocessing and statistical analyses of the imaging data were performed using the SPM12 (v7771) toolbox (Wellcome Trust Centre for

Neuroimaging, London, UK) as well as custom-made scripts running on MATLAB R2015a and MATLAB R2017a (The MathWorks Inc., Natick, MA, USA). For repeated measures ANOVA, we used the ranova method in the RepeatedMeasuresModel class included in the statistics toolbox of MATLAB R2017a. Permutation-based significance testing was completed using custom-made scripts in MATLAB R2017a.

2.3.2.3. ROI definition. A separate functional localiser run was used to determine face-selective visual cortical areas for each participant. Due to the well-known right-lateralisation of face processing (Kanwisher et al., 1997; McCarthy et al., 1997; Rossion et al., 2012; Zhen et al., 2015), we focused our analysis on the right hemisphere where these regions could be identified more reliably. The OFA (Pitcher et al., 2007) in the inferior occipital gyrus and the two subregions of the FFA located in the posterior-lateral and anterior-lateral tip of the mid-fusiform sulcus – called pFus-faces/FFA-1 and mFus-faces/FFA-2, respectively (Grill-Spector et al., 2017; Pinsk et al., 2009; Weiner and Grill-Spector, 2010) – were identified as areas showing higher fMRI responses to face than house images. To determine the locations of these ROIs for each participant, we used the individual face vs house contrast t-maps thresholded with a two-tailed voxel-level FDR at q = 0.05. In addition to these face-selective regions, a control visual cortical area selective for processing of body images, namely the extrastriate body area (EBA) (Downing et al., 2001) was also individually localised in the extrastriate visual cortex as an area showing higher fMRI responses to body than house images using the individual body vs house contrast t-maps thresholded with a two-tailed voxel-level FDR at q = 0.05.

It was possible to define the right mFus-faces/FFA-2 for 32 participants (MNI x, y, z coordinates mean ± standard error (SE) in mm: 40 ± 0.5, −47 ± 1.0, −19 ± 0.6) and the right pFus-faces/FFA-1 for 31 participants (MNI coordinates mean ± SE: 43 ± 0.9, −60 ± 0.9, −17 ± 0.7). The right OFA was found for 30 participants (MNI coordinates mean ± SE: 40 ± 0.7, −79 ± 1.2, −13 ± 0.6), and the right EBA could be defined for all participants (MNI coordinates mean ± SE: 50 ± 0.7, −72 ± 1.1, 4 ± 1.0).

In addition to the visual cortical regions, the PT-IFG was also individually localised as an area showing larger fMRI responses to probe stimulus in the case of face identity WM trials than grating orientation WM trials in the WM fMRI experiment, using the individual face identity WM vs grating orientation WM contrast t-maps thresholded with a two-tailed voxel-level FDR at q = 0.05. It was possible to define the right PT-IFG for 32 and the left PT-IFG for 27 participants (MNI coordinates mean ± SE: 47 ± 1.0, 22 ± 1.0, 25 ± 1.0 and −45 ± 1.1, 19 ± 0.8, 24 ± 0.8 for right and left hemisphere, respectively).

In the ANOVA model with ROI as within-subject factor we only included participants for whom we could define all the ROIs, while for correlation analyses, we used the data of all participants for whom we could define the investigated ROI.

2.4. Correlation analysis

For correlation analyses we used the Robust Correlation Toolbox v2 (Pernet et al., 2013) in MATLAB R2017a. Skipped Spearman's correlation coefficients (r_s) were calculated using the adjusted box-plot rule for bivariate outlier detection. The number of outliers (NO) is reported for each correlation. Two-tailed P values were derived from a bootstrap distribution (10,000 samples) with a lower limit of P = 0.0001. P values were corrected for multiple comparisons using the Holm-Bonferroni method within each hypothesis set and provided as $P_{c,N}$ with N marking the number of correlations corrected for when N > 1.

2.5. Behavioural data analyses

To investigate the participants' WM performance, we calculated d prime (d') scores by using the standardised difference between the hit rate and false alarm rate for each condition and each participant, where higher d' score indicated better performance. For second-level analyses we used a two-way repeated-measures ANOVA on d' scores with WM content (face identity WM vs grating orientation WM) and Distractor category (face distractor vs no distractor for the EEG experiment and face distractor vs grating distractor for the fMRI experiment) as within-subject factors. Significance testing was performed using the same permutation-based approach described in Section 2.3.2.2.

To characterize the participants' ability to resist face distractors – behavioural distractor resistance –, we used the face identity working memory performance (d') in face distractor trials of both the EEG and fMRI WM tasks after regressing out the performance in no-distractor trials measured in the EEG experiment to control for the confounding effect of the overall face identity WM ability of the participants. The participants' behavioural distractor resistance during EEG and fMRI recordings was then correlated with their neural EEG and fMRI distractor congruency effects, respectively, as well as with their working memory recall precision, measured independently using an orientation delayed-estimation task (Gorgoraptis et al., 2011; Manga et al., 2020).

2.6. Orientation delayed-estimation task

Participants of the EEG and fMRI experiments also completed a delayed-estimation task (Supplementary Fig. 1) in a previous study that has been recently published (Manga et al., 2020). The task was a modified, incentivised version of the orientation delayed-estimation task employed by Gorgoraptis et al. (2011). During the course of one trial of the task, three bars with different colour and orientation were presented consecutively at the centre of the screen (stimulus bars), followed by a probe bar appearing in a colour identical to one of the previously presented three bars (target bar). Participants were instructed to memorise all three stimulus bars, and then recall the orientation of the target bar (cued retrospectively) as accurately as possible by rotating the probe bar using the keyboard of the computer. At the beginning of each trial, a reward cue indicated whether small or large reward could be earned, however, in the current analysis data was not split by reward conditions. Thus, trials were categorised based on the position of the target bar in the stimulus sequence, resulting in three experimental conditions (recall 1st, 2nd and 3rd bar), with 144 trials per condition (for a detailed description of the task see Manga et al., 2020).

To quantify the quality of the visual working memory representations in the delayed-estimation task, angular deviation between the orientation of the target bar and the response was calculated for each trial (recall error), and the reciprocal of the circular SD of this recall error was used as an overall measure of performance, called recall precision (with higher recall precision values indicating better visual working memory performance).

3. Results

3.1. Congruency effects on the face-distractor-related EEG activity

3.1.1. Behavioural results

During the EEG recordings a significant Distractor category × WM content interaction ($F(1,32) = 5.82$, $P = 0.023$) was revealed as a result of reduced WM performance (Fig. 2a) in the case of the face delay distractor as compared to the no distractor condition in face identity WM trials ($P_{c,2} = 0.0011$), which was absent in grating orientation WM trials ($P_{c,2} = 0.47$). Furthermore, face identity WM performance was poorer than grating orientation WM performance, both in the presence ($P_{c,2} = 0.0001$) and absence of distractors ($P_{c,2} = 0.012$). Significant Distractor category × WM content interaction ($F(1,32) = 5.65$, $P = 0.023$) was also found for reaction times as a result of larger non-significant distractor effect in face identity WM trials (mean ± SD: 1099 ± 231 ms and 1070 ± 250 ms for the presence and absence of face distractors, respectively, $d = 0.38$, $P_{c,2} = 0.076$) relative to grating orientation WM

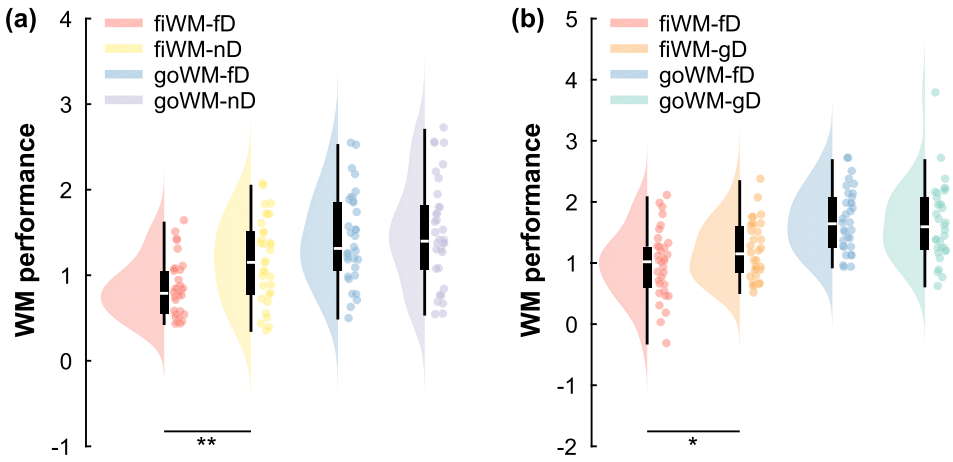

Fig. 2. Behavioural performance on the working memory task. Face identity and grating orientation WM performances (d' scores) are presented in the case of face and no distractor conditions in the EEG experiment (a) and in the case of face and grating distractor conditions in the fMRI experiment (b) using an in-house modified version of the RainCloudPlots tool (Allen et al., 2019). Probability distributions are depicted by split-half violin plot and dots represent individual data points. In each box-and-whisker plot the box represents the interquartile range (IQR) with lower and upper boundary lines at the 25th and 75th percentile of the data, respectively. Whiskers indicate the non-outlier (1.5 × IQR) range, and the white central line indicates the median of the data. Significant distractor effects are indicated by asterisks: $^{*}P < 0.05$, $^{**}P < 0.01$. Abbreviations: fiWM (face identity working memory), goWM (grating orientation working memory), fD (face distractor), gD (grating distractor), nD (no distractor), WM (working memory).

trials (mean ± SD: 1077 ± 230 ms and 1076 ± 250 ms for the presence and absence of face distractors, respectively, $d = 0.01$, $P_{c,2} = 1$).

Next, we explored the association between the participants' ability to resist face distractors – behavioural distractor resistance – in the face identity WM task performed during the EEG recordings and their independently measured working memory recall precision. The results revealed significant correlation between the participants' recall precision and behavioural distractor resistance ($r_s = 0.43$, $P = 0.029$, NO = 2), showing that the ability to resist congruent distractor interference in a face identity WM task is closely associated with recall precision (Supplementary Fig. 2a). Next, we performed the same correlation analysis separately for the recall precision measured in the case of the first, second and third item of the sample display. Significant correlation was found only for the second item ($r_s = 0.45$, $P_{c,3} = 0.049$, NO = 0), whereas correlation in the case of the first ($r_s = 0.34$, $P_{c,3} = 0.14$, NO = 1) and third ($r_s = 0.23$, $P_{c,3} = 0.23$, NO = 0) stimulus was non-significant.

3.1.2. EEG results

We focus our analysis on the EEG activity associated with the first face distractor (Fig. 3a). The reason for adding a second distractor was to avoid the building up of the neural processes associated with the anticipation of the test stimulus during the period of the first distractor-related response. Additionally, the processing of the second distractor might be confounded by test anticipatory processes as well as adaptation effects that are known to be most prominent at the N170 and N250 ERP components (Kovács et al., 2006; Webster and MacLeod, 2011), i.e. in a time window overlapping with SN.

Using cluster-based permutation testing we found significant frontal, central, parietal positive ($P_{cp} = 0.0004$) and occipital, occipito-temporal negative ($P_{cn} = 0.0002$) distractor congruency clusters corresponding to the contrast between the conditions with congruent and incongruent face distractor stimuli (Fig. 3b). The congruency effects' spatio-temporal properties within the early time interval (200–450 ms) in the current study closely corresponded to that previously described for SN and a positive component accompanying SN, the so-called selection positivity (SP) (Hillyard and Anllo-Vento, 1998). Although, the SN/SP components in the current experiment formed part of a more extended continuous significant congruency effect cluster, the scalp topography suggests that the early SN/SP might be differentiated from the later segment of the cluster, starting from around 450 ms and corresponding to the P3b component of the ERP responses (Polich, 2007).

The early P1 and N1 ERP components were not affected by distractor congruency. Because a previous study found distractor congruency effects on the N170 component of the face-distractor-related responses using a more traditional analysis of the EEG data (Sreenivasan and Jha, 2007), we also performed a peak detection-based analysis of the N170 component on our dataset (Supplementary text 2). The results – in agreement with our cluster-based analysis – indicated no significant congruency effects on the N170 component latency ($F(1,29) = 0.16$, $P = 0.72$) and amplitude ($F(1,29) = 0.09$, $P = 0.80$).

We also performed a correlation analysis to test the relationship between the participants' behavioural distractor resistance and the strength of SN congruency effect. The results revealed a significant positive correlation between behavioural distractor resistance and the congruency effects measured within the SN time interval ($r_s = 0.51$, $P_{c,2} = 0.008$, NO = 2): WM performance was more impaired in congruent face distractor trials in those participants who showed larger SN (Supplementary Fig. 4a). On the other hand, we failed to find significant correlation between behavioural distractor resistance and the EEG congruency effect measured in a later (450–700 ms) time interval, corresponding to P3b ($r_s = 0.28$, $P_{c,2} = 0.11$, NO = 1).

Testing the effect of distractor congruency on post-stimulus alpha power time course revealed significant reduction of post-stimulus alpha power time course following congruent as compared to incongruent distractors (Fig. 4). This congruency effect started on parieto-occipital electrodes and around 600 ms extended to right-hemisphere frontolateral electrodes. The right hemisphere lateralised significant negative cluster ($P_{cn} = 0.0344$) started in Pz, P2, POz, PPO2h parietal electrodes at 346 ms and ended in the right frontal region (F8, FT8, F10) at 950 ms. These findings are in concordance with the results of our exploratory experiment showing significant congruency effects of post-stimulus alpha power time course in the case of both face- and grating-distractor-related EEG activity (see Supplementary text 1 and Supplementary Fig. 5).

The traditional analysis we performed to investigate congruency effect on post-stimulus alpha power ignores the fact that electrophysiological signals exhibit both periodic and aperiodic properties. However, recent findings show that the aperiodic component of the EEG signal can reflect physiological information (Gao et al., 2017; He et al., 2010; Podvalny et al., 2015) and failing to disentangle periodic from aperiodic activity may lead to compromised interpretations (Donoghue et al., 2020). In order to specifically investigate periodic activity, we used a model fitting approach in the spectral domain, which allowed us to separate the periodic and aperiodic components of post-stimulus alpha power. We found significant effect of distractor congruency on post-stimulus total alpha power following distractor onset on rightward lateralized posterior ($P_{cn1} = 0.01$), left frontal ($P_{cn3} = 0.048$) and right frontal ($P_{cn2} = 0.046$) electrode clusters, with reduced post-stimulus total alpha power in the congruent distractor condition (see Fig. 5). When investigating the distractor congruency effect on the periodic component of post-stimulus alpha power, we revealed two significant clusters

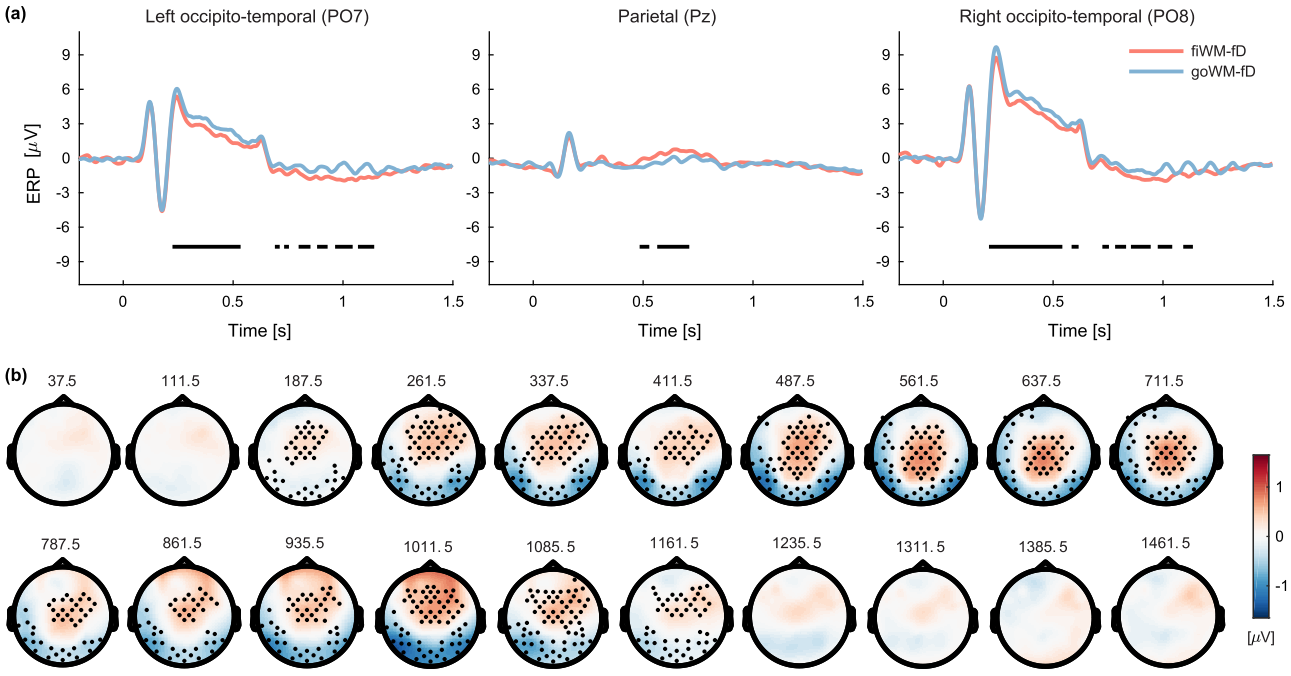

Fig. 3. The effects of face distractor congruency on event-related potentials. The time course of grand average occipito-temporal and parietal event-related potentials (ERPs) evoked by the first face distractor is presented for both congruent and incongruent conditions (a). Horizontal black lines below the time courses indicate significant face distractor congruency effects at sample points that belong to significant clusters. Spatio-temporal effects of first distractor congruency on EEG are shown in panel (b) for the time interval between 0 s and 1.5 s. A significant negative cluster started at 208 ms in right occipito-temporal electrodes (PO10, PO8, PPO10h), and ended at 1160 ms in the left occipito-temporal region (PO9, PO7, PPO9h). The positive cluster overlapped in time with the negative cluster, it started at 204 ms in left central electrodes (Cz, C1, CCP1h) and ended in a broader right fronto-central scalp region (C4, F6, FC4, C6, FFC6h, FCC4h, FTT8h) at 1146 ms. These findings are in close agreement with the results of our exploratory experiment (see Supplementary text 1 and Supplementary Fig. 3). Topographic plots stand for the difference of baseline-corrected ERPs between congruent and incongruent face distractor conditions (face identity WM – face distractor vs grating orientation WM – face distractor) averaged in 75 ms wide time windows with window centres indicated in ms above the plots. Hot colours indicate more positive-going ERP activity for the face identity WM – face distractor condition. Black dots mark EEG electrodes with significant face distractor effect found for at least one sample point within the corresponding time intervals. Abbreviations: fiWM (face identity working memory), goWM (grating orientation working memory), fD (face distractor).

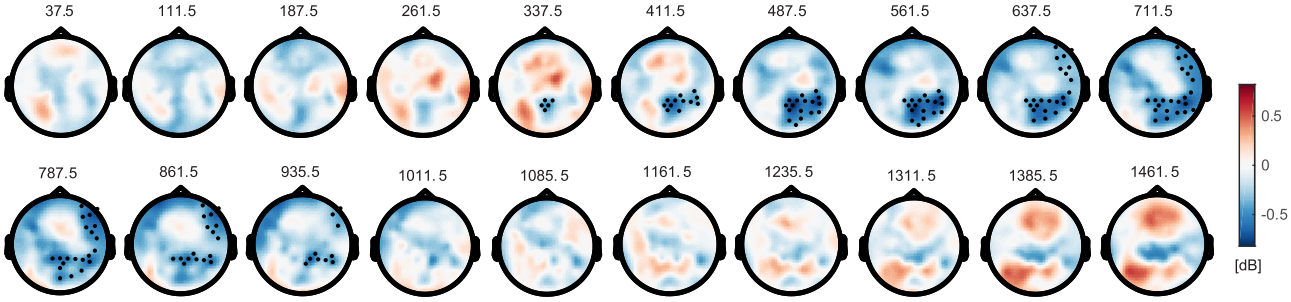

Fig. 4. The effects of face distractor congruency on alpha power time course. Spatio-temporal effects of face distractor congruency on the power of evoked alpha oscillations ($10\log_{10}P_{\alpha bc}$) are shown for the time interval between 0 s and 1.5 s after the onset of face distractor stimuli. Topographic plots stand for the difference of grand average alpha power between congruent and incongruent distractor conditions (face identity WM – face distractor vs grating orientation WM – face distractor) averaged in 75 ms wide time windows with window centres indicated in ms above the plots. Cold colours indicate more negative-going baseline-corrected alpha power values for the face identity WM – face distractor condition. Black dots mark EEG electrodes with significant face distractor effect found for at least one sample point within the corresponding time windows. Abbreviations: dB (decibels).

in posterior (P_{cn2} = 0.038) and right frontal (P_{cn1} = 0.026) regions, largely overlapping with the significant clusters revealed for total alpha power. Finally, we found significant (P_{cn} = 0.013) distractor congruency effect on the aperiodic component of post-stimulus alpha power on a right posterior electrode cluster. Importantly, behavioural distractor resistance correlated significantly with the significant posterior distractor congruency effect on post-stimulus periodic alpha power (r_s = −0.40, $P_{c,2}$ = 0.028, NO = 3, see Supplementary Fig. 4b) but not with the significant distractor congruency effect on post-stimulus aperiodic alpha power (r_s = −0.16, $P_{c,2}$ = 0.42, NO = 2).

3.2. Congruency effects on the distractor-related fMRI responses

3.2.1. Behavioural results

In agreement with the results of the main EEG and exploratory EEG (see Supplementary text 1) experiments, WM performance (Fig. 2b) was reduced in the case of face as compared to grating distractors (no-distractors in the main EEG experiment) in face identity ($P_{c,2}$ = 0.049) but not in grating orientation WM trials ($P_{c,2}$ = 0.88), although the interaction of WM content and Distractor category did not reach statistical significance (F(1,32) = 2.93, P = 0.098). In addition, there was a signif-

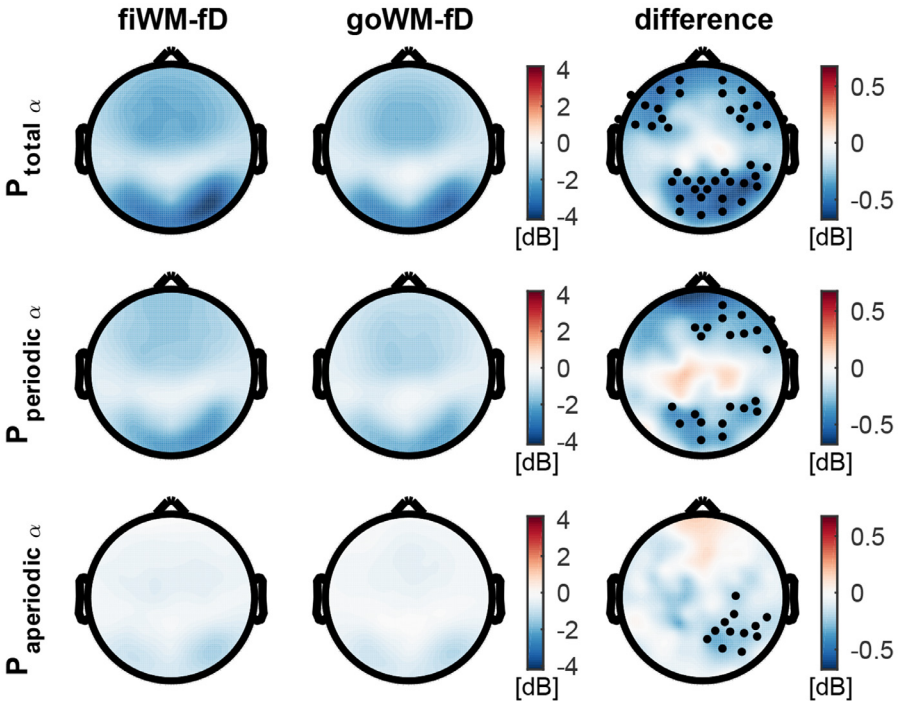

Fig. 5. The effect of facedistractor congruency on alpha power. Grand average post-stimulus alpha power ($P_{total\ \alpha}$, first row), its periodic ($P_{periodic\ \alpha}$, second row) and aperiodic ($P_{aperiodic\ \alpha}$, last row) components derived from the 350–950 ms time range after the onset of face distractor stimuli. Topographies are shown for face identity WM – face distractor (fiWM-fD) and grating orientation WM – face distractor (goWM-fD) conditions as well as for their difference (fiWM-fD vs goWM-fD). Black dots on difference topographies mark significant electrodes. Abbreviations: dB (decibels).

icant main effect of the WM content ($F(1,32) = 32.97$, $P = 0.0001$): WM performance, similarly to our main EEG experiment, was poorer when face identity information was maintained in WM in the cases of both distractor conditions.

Importantly, in accordance with the results of our EEG experiment, behavioural distractor resistance in the congruent face delay distractor condition positively correlated with the participants' recall precision ($r_s = 0.61$, $P = 0.0006$, NO = 2, see Supplementary Fig. 2b) and this association was driven by the strong correlation between behavioural distractor resistance and the recall precision measured in the cases of the first ($r_s = 0.62$, $P_{c,3} = 0.0006$, NO = 2) and second item ($r_s = 0.56$, $P_{c,3} = 0.0016$, NO = 1), but not the third item ($r_s = 0.30$, $P_{c,3} = 0.11$, NO = 0). Reaction times were not affected by distractor category ($F(1,32) = 1.40$, $P = 0.25$), WM content ($F(1,32) = 0.14$, $P = 0.72$), or their interaction ($F(1,32) = 0.65$, $P = 0.44$).

3.2.2. *fMRI results*

3.2.2.4. Whole brain analysis. In agreement with our prediction, whole-brain analysis of the fMRI data revealed stronger fMRI responses for congruent as compared to incongruent face distractors in the bilateral ventral occipito-temporal cortex, including the fusiform gyrus as well as in the vlPFC, being most prominent in the PT-IFG (Fig. 6). In the case of grating distractors, the most pronounced congruency-induced fMRI response enhancements were found bilaterally in the superior and inferior parietal cortex, superior frontal gyrus as well as in the precentral gyrus (Supplementary Fig. 6, see also Supplementary Table 2). Overall, these results are in accordance with the extensive previous research showing that ventral areas of the PFC co-operate with the ventral temporal cortex to support object WM (Courtney et al., 1998, 1997; Nee et al., 2013; Nee and D'Esposito, 2018). On the other hand, dorsal areas of the PFC and the parietal cortex play a central role in spatial WM as well as in the maintenance of orientation information (Courtney et al., 1998, 1997; D'Esposito et al., 1998; Nee et al., 2013; Nee and D'Esposito, 2018; Serences, 2016).

3.2.2.5. Congruency effects in the visual cortical ROIs. To investigate congruency effects in the visual cortical processing of distractors, we individually identified three face-selective areas in the occipito-temporal cortex – namely OFA, pFus-faces/FFA-1, and mFus-faces/FFA-2 – and a control visual cortical area selective for the processing of body images in the extrastriate visual cortex – namely EBA – using an independent localiser. Due to the well-known right-lateralisation of face processing (Kanwisher et al., 1997; McCarthy et al., 1997; Rossion et al., 2012; Zhen et al., 2015), we focused our analysis on the right hemisphere where face-selective regions could be identified more reliably.

The ROI analysis (Fig. 7) revealed that distractor congruency effect – enhanced fMRI responses to congruent as compared to incongruent distractors – differed between visual cortical regions (WM content × Distractor category × ROI interaction: $F(3,81) = 7.80$, $P = 0.0002$). In the mFus-faces/FFA-2, significant WM content × Distractor category interaction ($F(1,27) = 16.51$, $P = 0.0003$) was revealed, which is explained by a strong distractor congruency effect (face identity vs grating orientation WM) on fMRI responses to face ($P_{c,2} = 0.0004$) but not to grating distractors ($P_{c,2} = 0.96$). Whereas in the case of pFus-faces/FFA-1, both distractors evoked larger fMRI responses when they were congruent (face distractor: $P_{c,2} = 0.004$, grating distractor: $P_{c,2} = 0.0059$) leading to significant WM content × Distractor category interaction ($F(1,27) = 27.72$, $P = 0.0001$) as a consequence of congruency coded with opposite contrasts for the two distractor conditions in our design. Distractor congruency had no significant effect on fMRI responses either in the OFA ($F(1,27) = 2.16$, $P = 0.16$) or in the EBA ($F(1,27) = 0.25$, $P = 0.63$).

To further investigate the effect of distractor category, we tested the Distractor category × ROI interaction for each level of WM content. The Distractor category × ROI interaction was significant in both the face identity ($F(3,81) = 27.44$, $P = 0.0001$) and grating orientation WM conditions ($F(3,81) = 18.14$, $P = 0.0001$): face as compared to grating distractors evoked significantly larger fMRI responses in all face-selective ROIs ($d > 0.97$, $P_{c,4} = 0.0001$ for both WM conditions), whereas the distractor category effect on fMRI responses was weaker or non-significant in the EBA ($d = 0.61$, $P_{c,4} = 0.0032$ for grating orientation WM and $d = 0.29$, $P_{c,4} = 0.36$ for face identity WM).

3.2.2.6. Congruency effects in the pars triangularis of the IFG. Besides the visual cortical ROIs, distractor congruency effects were also explored in the PT-IFG. This region was localised individually from the fMRI responses to probe displays using the face identity WM vs grating orienta-

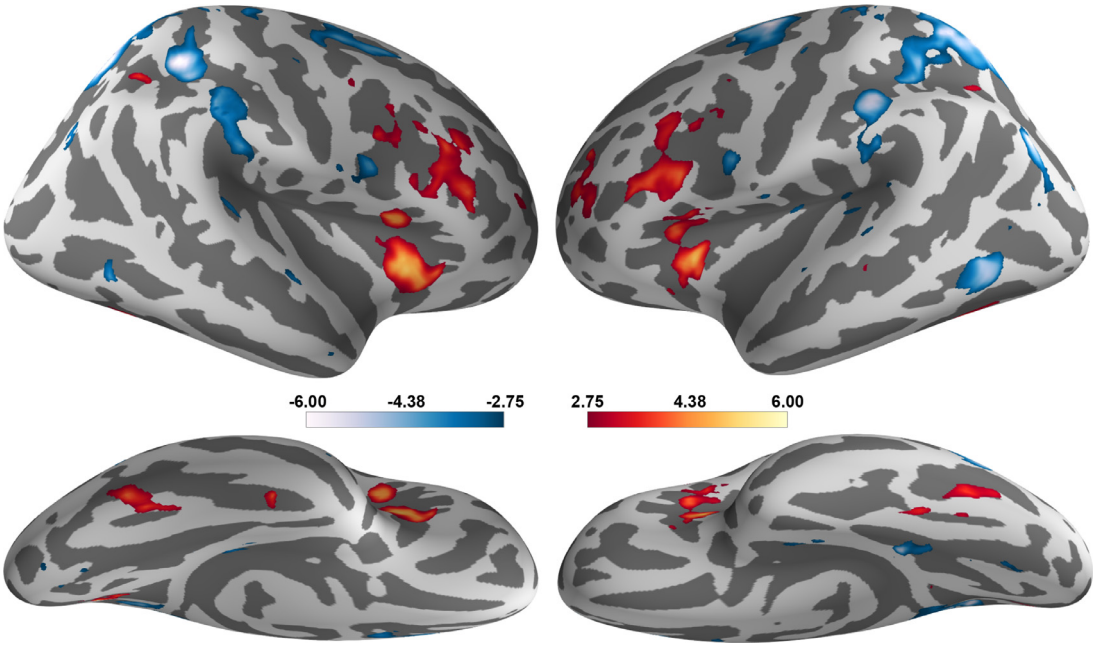

Fig. 6. Surface map of positive and negative congruency effect on fMRI responses to face distractors. Surface-projected (Wu et al., 2018) second-level statistical t-map of congruent vs incongruent face distractor (face identity WM – face distractor vs grating orientation WM – face distractor) contrast was displayed in lateral (top) and ventral (bottom) view using a two-tailed FDR-corrected threshold (P = 0.0048). Hot colours indicate significantly higher fMRI responses to congruent as compared to incongruent face distractors (i.e. positive congruency effect), while cold colours indicate significantly higher fMRI responses to incongruent as compared to congruent face distractors (i.e. negative congruency effect). The full list of brain regions showing significant positive and negative congruency effects in case of face distractors is presented in the Supplementary Table 1.

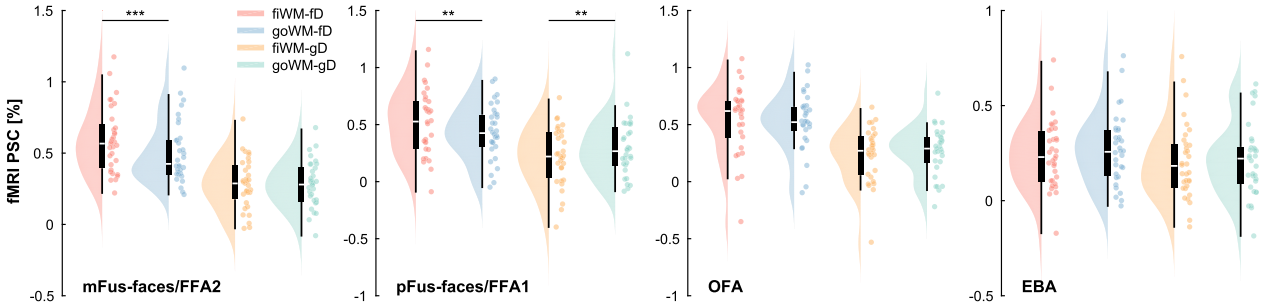

Fig. 7. Distractor congruency effects in the visual cortical ROIs. fMRI percent signal change evoked by face and grating distractors are presented for both congruent and incongruent conditions in each visual cortical region of interest (ROI) using an in-house modified version of the RainCloudPlots tool (Allen et al., 2019). Probability distributions are depicted by split-half violin plot and dots represent individual data points. In each box-and-whisker plot the box represents the interquartile range (IQR) with lower and upper boundary lines at the 25th and 75th percentile of the data, respectively. Whiskers indicate the non-outlier (1.5 × IQR) range, and the white central line indicates the median of the data. Significant congruency effects are indicated by asterisks: **P<0.01, ***P<001. Abbreviations: PSC (percent signal change), fiWM (face identity working memory), goWM (grating orientation working memory), fD (face distractor), gD (grating distractor), mFus (mid fusiform), pFus (posterior fusiform), FFA (fusiform face area), OFA (occipital face area), EBA (extrastriate body area).

tion WM contrast. In our task, participants were required to encode and store the identity of two different faces on each trial. This entailed that during the presentation of the probe stimuli, matching mnemonic and probe information involved attentional selection and prioritisation of memorandum representations. Furthermore, using superimposed face and grating images as probe displays ensured that WM-content-based response modulation of this IFG region was associated with top-down attentional selection processes. Importantly, the location of the PT-IFG ROI identified based on the fMRI responses to the probe display closely overlapped with the location of the PT-IFG congruency effect found in the case of face-distractor-related fMRI responses (distractor-related group peak/probe-related ROI average MNI coordinates (in mm) are $x = -44/-45$, $y = 18/19$, $z = 28/24$ for the left PT-IFG and $x = 48/47$, $y = 22/22$, $z = 24/25$ for the right PT-IFG).

We found significant WM content × Distractor category interaction ($F(1,26) = 26.95$, $P = 0.0002$), not modulated by the ROI (left and right PT-IFG) factor (WM content × Distractor category × ROI interaction: $F(1,26) = 0.20$, $P = 0.66$). fMRI responses were significantly increased when face identity information was actively maintained in WM as compared to grating orientation in the presence of face ($P_{c,2} = 0.0001$) but not grating distractors ($P_{c,2} = 0.90$) (Fig. 8). These results thus clearly show that distractor congruency effects in the PT-IFG are present only in the case of face distractors. Furthermore, face distractors evoked larger fMRI responses than grating distractors in the congruent ($P_{c,2} = 0.0001$) but not in the incongruent condition ($P_{c,2} = 0.79$).

3.2.2.7. Relationship between fMRI distractor congruency effects end behavioural distractor resistance. We investigated the relationship between the participants' behavioural distractor resistance measured in the congruent face delay distractor condition during the fMRI experiment and the strength of fMRI congruency effect measured for face delay distractors in the left and right PT-IFG, right mFus-faces/FFA-2 and right

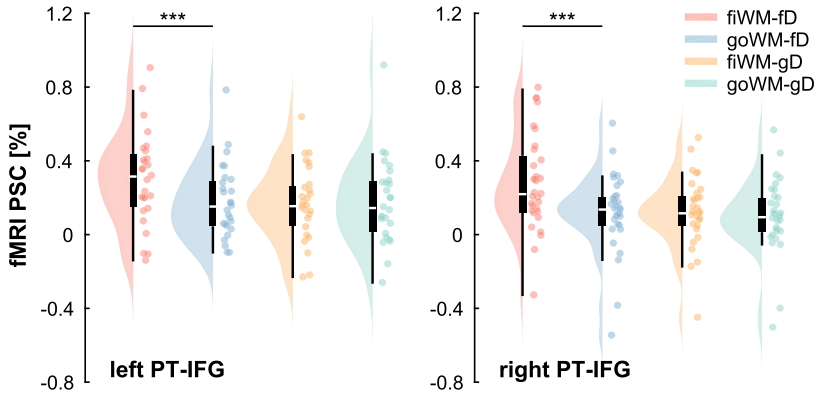

Fig. 8. Distractor congruency effects in the pars triangularis of the IFG. fMRI percent signal change evoked by face and grating distractors are presented for both congruent and incongruent conditions in left and right PT-IFG ROIs using an in-house modified version of the RainCloudPlots tool (Allen et al., 2019). Probability distributions are depicted by split-half violin plot and dots represent individual data points. In each box-and-whisker plot the box represents the interquartile range (IQR) with lower and upper boundary lines at the 25th and 75th percentile of the data, respectively. Whiskers indicate the non-outlier (1.5 × IQR) range, and the white central line indicates the median of the data. Significant congruency effects are indicated by asterisks: ***P<001. Abbreviations: PSC (percent signal change), fiWM (face identity working memory), goWM (grating orientation working memory), fD (face distractor), gD (grating distractor), PT-IFG (pars triangularis of the inferior frontal gyrus), ROI (region of interest).

pFus-faces/FFA-1, i.e. in regions where significantly larger fMRI responses to congruent as compared to incongruent face distractors were found. A significant positive correlation was found in the case of the right PT-IFG (r_s = 0.53, $P_{c,4}$ = 0.0024, NO = 0, see Supplementary Fig. 7a): greater increase of fMRI responses to congruent as compared to incongruent face distractors in this region indicated better face identity WM performance in face distractor trials. The obtained association between behavioural distractor resistance and fMRI responses in the right PT-IFG was specific to the distractor-related neural processes because our additional analysis revealed no significant correlation between behavioural distractor resistance and WM-content-dependant modulation of the fMRI responses either in the retro-cue- or in the probe-related fMRI activity ($P_{c,2}$ > 0.46 for all correlations). Furthermore, distractor congruency effect in the left PT-IFG (r_s = 0.27, $P_{c,4}$ = 0.39, NO = 1), right mFus-faces/FFA-2 (r_s=0.38, $P_{c,4}$ = 0.09, NO = 0) and right pFus-faces/FFA-1 (r_s = 0.11, $P_{c,4}$ = 0.52, NO = 0) did not show significant correlation with the participants' behavioural distractor resistance.

3.2.2.8. Relationship between fMRI and EEG distractor congruency effects. We also performed a correlation analysis to test the relationship between the significant face delay distractor congruency effect on fMRI responses in the left and right PT-IFG, right mFus-faces/FFA-2 and right pFus-faces/FFA-1 and the strength of the congruency effect in the case of SN and post-stimulus periodic alpha power. The results revealed that the right PT-IFG congruency effect showed a significant negative correlation with the congruency effect measured on the post-stimulus periodic alpha power (r_s = −0.62, $P_{c,8}$ = 0.0008, NO = 1): greater reduction of post-stimulus periodic alpha power following congruent as compared to incongruent face distractors indicated greater increase of fMRI responses to congruent as compared to incongruent face distractors (Supplementary Fig. 7b). Furthermore, the congruency effect in the right PT-IFG was not associated with SN congruency effect (r_s = 0.32, $P_{c,8}$ = 0.64, NO = 5). In the case of the left PT-IFG, right mFus-faces/FFA-2 and rigth pFus-faces/FFA-1, fMRI congruency effect did not correlate with the EEG congruency effects ($P_{c,8}$ > 0.33 for all correlations).

These results are in agreement with previous research revealing strong correlation between BOLD signal and alpha oscillations in local field potentials in the visual cortex (Conner et al., 2011; Hermes et al., 2017) as well as a close association between attentional modulation of the visual cortical fMRI activity and post-stimulus alpha power but not the early ERP components (P1, N1, N250) (Itthipuripat et al., 2019). It is also in accordance with an earlier study showing that BOLD signal within the dorsal attentional network correlates with the occipital alpha power (Zumer et al., 2014).

4. Discussion

The behavioural results showed that participants' ability to resist congruent distractors during face identity WM maintenance positively correlated with their WM recall precision, measured independently using an orientation delayed-estimation task. Our EEG results revealed selection negativity in congruent as compared to incongruent face-distractor-related ERP responses and the magnitude of SN showed a negative association with the participants' behavioural distractor resistance. These findings provide support for WM-content-guided proactive attentional selection processes that enhance early processing of external distractors and thus hamper distractor resistance. Furthermore, our fMRI experiment showed significant face-distractor-related congruency effects in the mFus-faces/FFA-2 and the PT-IFG, which in the case of PT-IFG was significantly correlated with the participants' behavioural distractor resistance as well as with the congruency effect on post-stimulus periodic alpha power. These fMRI results suggest that top-down attentional control processes originating from the PT-IFG are engaged in the protection and separation of memorandum representation from the distractor representation within visual cortical areas retaining the most selective mnemonic code.

The behavioural results revealed reduced face identity WM performance in the presence of face distractors, which is in accordance with previous findings (Clapp et al., 2010; Sreenivasan and Jha, 2007; Yoon et al., 2006) showing that distractors that match the WM content will cause interference when fine detail information – allowing no abstract level coding – must be stored in WM. On the other hand, grating distractors failed to have a significant effect on orientation WM performance. One possible explanation for this is that orientation information might have been maintained using spatial attention markers (Bae and Luck, 2017; Girshick et al., 2011), or alternatively, via a more abstract, verbal strategy making it less prone to interference (van Ede et al., 2019). Moreover, it might also be the case that grating distractors did have a biasing effect on the orientation WM mnemonic representations (Lorenc et al., 2018), although the size of this modulation might have been too small to be revealed by the delayed orientation match-to-sample task.

Furthermore, we showed that the participants' ability to resist congruent distractors during face identity WM maintenance in both our EEG and fMRI experiment positively correlated with their WM recall precision, measured independently using an orientation delayed-estimation task (Gorgoraptis et al., 2011; Manga et al., 2020). The same correlation analysis performed separately for the recall precision measured in the cases of the three items of the sample display revealed an association between fMRI behavioural distractor resistance and recall precision for the first and second items, as well as between EEG behavioural distractor resistance and recall precision for the second item, whereas correlation in the case of the third item was non-significant for either EEG or fMRI behavioural distractor resistance. This appears to be in agreement with the results of previous research investigating serial position effects in an orientation delayed-estimation task (Gorgoraptis et al., 2011), showing that earlier items are affected by interference between WM representations more strongly, whereas the last item of the sample display is

less affected, leading to the well-known recency effect in visual memory (Broadbent and Broadbent, 1981). Furthermore, our behavioural results are also in line with the findings of an earlier study (Nee and Jonides, 2008) showing that access to the mnemonic representation of the first and second item, but not the third item of the sample display leads to activation of the ventrolateral prefrontal cortex. Taken together, our findings provide strong support for a close functional association between the top-down attentional control processes underlying selection and mitigation of interference between competing WM representations in the case of different visual objects or features.

Our results provide the first electrophysiological evidence for early attentional selection of task-irrelevant delay distractor objects matching the memorandum category by revealing a significant SN in the distractor-related ERP responses. SN is a broad negative-going ERP component that is generated by non-spatial proactive attentional selection of visual features and shapes (Hillyard and Anllo-Vento, 1998; Keil and Müller, 2010; Kenemans et al., 1993; Previc and Harter, 1982; Smid et al., 1999). Therefore, our findings showing congruency-driven SN in ERP responses to irrelevant external distractors are in line with previous behavioural studies (Olivers et al., 2011, 2006; Soto et al., 2008) demonstrating WM-content-guided automatic allocation of visual attention in visual search tasks performed during the WM maintenance period, as reflected in faster reaction times for search targets matching the WM content. In the current study, SN started from ~200 ms after stimulus onset and no congruency effects were found on the P1 and N170 components of the ERP responses, which is in accordance with a large body of previous studies investigating SN in the case of attentional selection of visual feature conjunctions and shapes (Hillyard and Anllo-Vento, 1998; Keil and Müller, 2010; Kenemans et al., 1993; Previc and Harter, 1982; Smid et al., 1999). However, our results are at odds with the findings of an earlier EEG study (Sreenivasan and Jha, 2007) showing that N170 amplitudes of the ERP responses to congruent delay distractors are reduced as compared to the incongruent distractors and suggesting an early suppression of visual processing of irrelevant distractors matching the WM content. A major difference between the cited and the current study is that we used retro-cueing to indicate which encoded object category has to be matched to the probe stimulus on a given trial, to ensure that encoding of the sample stimuli does not differ between the face identity and grating orientation WM conditions and thus the modulation of delay distractor processing originates exclusively from top-down object-based attentional processes. On the other hand, in the study by Sreenivasan and Jha (2007) task-relevant object category was cued at the beginning of the trial and therefore it cannot be excluded that congruency effects on the N170 component could have originated from differences in object-specific adaptation processes (Kovács et al., 2006; Webster and MacLeod, 2011) during encoding between the congruent and incongruent trials. Importantly, in agreement with our prediction we also found that the magnitude of SN negatively correlates with the participants' ability to resist the interference caused by congruent face distractors. This is in line with the results of previous research suggesting that stronger neural responses to distractors are associated with larger distractor interference (Clapp et al., 2010; Gazzaley, 2011; Gazzaley et al., 2005). Taken together, our EEG results provide experimental support for WM-content-guided attentional selection of distractor objects sharing the memorandum category that in turn hampers distractor resistance. It is important to note that our EEG findings are also consistent with previous theoretical and experimental research that proposed the existence of WM match filter template in sensory areas (Hayden and Gallant, 2009; Myers et al., 2015; Nobre and Stokes, 2019; Sugase-Miyamoto et al., 2008) that computes the perceptual similarity between incoming sensory signals and an internal template, resulting in enhanced neural responses and attentional capture of task-irrelevant matching stimuli.

Our results revealed enhanced face-distractor-related fMRI responses in the bilateral PT-IFG when face identity as compared to grating orientation information had to be maintained in WM. No similar modulation was found in PT-IFG fMRI responses in the case of grating distractors, suggesting that it is not the retro-cue-induced sustained delay response that leads to enhanced face-distractor-related fMRI responses in PT-IFG in the congruent condition. Furthermore, the significant positive correlation that was revealed between the right PT-IFG congruency effects and the participants' behavioural distractor resistance provides additional strong support that congruency-induced PT-IFG activation might reflect neural processes involved in the mitigation of distractor interference. These findings are in accordance with earlier studies where using pre-cueing the authors found increased fMRI responses to congruent face delay distractors in the vlPFC (Dolcos et al., 2007; Jha et al., 2004) without elevated sustained delay activity in this region (Jha et al., 2004) as well as a positive association between the congruency-induced modulation of fMRI responses in this region and the participants' overall WM performance during the scans. Additionally, enhanced IFG activity in response to congruent visual objects was also reported in a recent retro-cueing fMRI study (Gayet et al., 2017). Several lines of experimental evidence suggest that the vlPFC might play a central role in selecting task-relevant memorandum information amidst competition (Myers et al., 2017; Nee et al., 2013). It has been shown that while there is a considerable overlap in the frontoparietal control network underlying attentional selection during perception and retro-cue-induced prioritisation of mnemonic information, the vlPFC is selectively activated in the latter but not in the former case (Lepsien and Nobre, 2007; Myers et al., 2017; Nee et al., 2013; Nee and Jonides, 2008). Furthermore, previous research (Jonides and Nee, 2006; Nee et al., 2013) provided converging evidence for the key role of vlPFC in the resolution of proactive interference in WM, i.e. the mitigation of the interference from previously relevant material, including mnemonic representations. Although, in these previous studies the left vlPFC was found to be more prominently activated than the right vlPFC in tasks involving prioritisation of mnemonic representations and proactive interference resolution, a meta-analysis of executive components of WM (Nee et al., 2013) revealed that it is the right PT-IFG that showed the most consistent activations when resistance of interference from intrusive irrelevant memory representations was investigated. Interestingly, the meta-analysis failed to reveal an association between PT-IFG (or other vlPFC regions) and mitigation of interference from external incongruent distractors having distinct neural representation as compared to the memorandum. In this case, the most consistent activations related to external distractor resistance were found in the dorsal frontoparietal attentional control regions, including the caudal superior frontal sulcus, superior parietal lobule and the intraparietal sulcus. Taken together, these previous findings suggest that the congruency-driven activation of PT-IFG in the case of face distractors in the present study might imply that preventing interference from irrelevant face distractors during face identity WM involves top-down attentional selection and protection of task-relevant mnemonic representations from the distractor representations.

Additionally, our results also revealed that congruency effects on PT-IFG show a significant correlation with the congruency effects found on post-stimulus periodic alpha power but not with that on the earlier SN. Previous research provided converging evidence that post-stimulus alpha power reduction reflects allocation of feedback attentional resources to visual information processing within the visual cortex (Itthipuripat et al., 2019; Scheeringa et al., 2016; Zumer et al., 2014). Moreover, stronger post-stimulus alpha power reduction is associated with enhanced stimulus processing (Bacigalupo and Luck, 2019; Van Diepen et al., 2016; Vanni et al., 1997) and increased fidelity of visual cortical perceptual and memory representations (Griffiths et al., 2019). The onset of the congruency effects on post-stimulus alpha power time course was delayed by about 150 ms as compared to that in the case of SN, which is consistent with the results of previous findings (Griffiths et al., 2019; Van Diepen et al., 2019) and suggests that post-stimulus alpha power congruency effects might reflect reactive allocation of attentional resources. Additionally, similarly to the PT-IFG, the strength of the congruency effect on post-stimulus periodic alpha

power showed a significant positive association with the participants' behavioural distractor resistance, as opposed to the negative association found between the magnitude of SN congruency effects and behavioural distractor resistance. Taken together, these results suggest that congruency effect on post-stimulus alpha power might reflect top-down attentional control processes originating from the PT-IFG and reactively allocated to the protection and separation of memorandum representation from the distractor representation.

By focusing our analysis on the IFG we did not mean to imply that other frontal and parietal regions could not have contributed to distractor resistance in our task conditions. In fact, we found congruency-driven activations in the bilateral mid-dlPFC that has previously been shown to be involved in distractor resistance (Feredoes et al., 2011; Sakai et al., 2002). However, in the current study mid-dlPFC activations were less prominent than those in the IFG and their location differed in the cases of the distractor- and probe-related fMRI responses, precluding the possibility to perform a ROI-based analysis for these regions. Additionally, a meta-analysis of external and internal distractor interference resistance (Nee et al., 2013) found modest support for the involvement of mid-dlPFC, which according to the authors might have been due to the fact that in the investigated studies – just as in the case of the current study – all contrasts included high-level control conditions and thus experimental and control conditions were matched for demands in higher executive functions (e.g. context and rule representations).

To assess how visual cortical information processing is modulated by congruency-driven top-down attentional processes, we investigated fMRI responses in the face-selective cortical areas, including the OFA in the inferior occipital gyrus as well as two distinct regions of the FFA within the mid-fusiform gyrus, corresponding to pFus- and mFus-faces (also known as FFA-1 and FFA-2) overlapping the posterior-lateral and anterior-lateral tip of the mid-fusiform sulcus, respectively. OFA might considered to be an entry node of the face recognition network primarily involved in the visual analysis of individual facial features, whereas FFA is specialised for the selective coding of face identity through constructing more complex holistic/configural representations (Grill-Spector et al., 2017; Yovel, 2016). The results revealed congruency effects within the two subregions of the FFA, but not in the OFA. Furthermore, congruency effect differed between the two FFA subregions. In the mFus-faces/FFA-2 – similarly to the IFG – congruency effects were present only in the case of face distractors, whereas in the pFus-faces/FFA-1 congruency effects were present in the case of both distractors: fMRI responses were enhanced in the case of congruent face and grating distractors as compared to the incongruent ones. These differences in congruency effect could be explained by the cytoarchitectonical and functional differences found between the two FFA subregions (Grill-Spector et al., 2017; Stigliani et al., 2019; Weiner et al., 2010) as well as by the proximity to (and thus partial overlap with) nearby object-selective regions in the ventral occipito-temporal cortex (Grill-Spector et al., 2001) in the case of pFus-faces/FFA-1. Taken together, these findings imply that mFus-faces/FFA-2 might play a key role in face identity WM as well as suggest that modulation of information processing within the visual cortex by congruency-driven top-down attentional processes might take place most prominently in face-selective visual cortical areas retaining the most selective mnemonic code.

It is important to acknowledge that in both our EEG and fMRI experiments overall face identity WM performance was lower than grating orientation WM performance, raising the possibility that this might have affected the obtained congruency effects. However, there are several reasons why we think this possibility can be excluded. First, we found SN and post-stimulus alpha power congruency effects in both face- and grating-distractor-related EEG activity also in our exploratory EEG experiment (see Supplementary text 1), even though there was no difference between face identity and grating orientation WM performance. Although the SN effects became only marginally significant after the final correction for multiple comparisons, all these results speak strongly against an explanation that EEG congruency effects obtained in our main experiment are based on the difference in task performance or maintained object category. Additionally, our previous research showed that task difficulty – face gender discrimination performance – does not affect ERP responses to face stimuli within the time window of the SN (Bankó et al., 2011). Second, congruency-driven fMRI response enhancements in both the PT-IFG and the mFus-faces/FFA-2 were present only in the case of face but not grating distractors, suggesting that the difference in face identity and grating orientation WM performance alone did not modulate fMRI activity in these regions. Furthermore, we found no congruency effects in the EBA, a control visual cortical area selective for the processing of body images. This implies that face identity and grating orientation WM performance differences did not affect overall visual cortical responses to delay distractors. Third, the correlation between fMRI congruency effects and behavioural distractor resistance was restricted to the distractor-related neural responses. No significant association was found in the case of WM-content-based modulation of retrocue- and probe-related fMRI responses. Fourth, we performed the EEG and fMRI analysis selectively on the correct trials (the results are not presented) and obtained very similar results as those found in the cases of all trials, with a moderate effect size reduction as a consequence of decreased trial numbers.

5. Conclusions

In sum, our findings reveal two top-down attentional control processes affecting distractor resistance during WM maintenance. First, WM-content-guided proactive early attentional selection of matching distractors that is reflected in congruency-driven SN and impairs interference resistance. Second, reactive top-down attentional control processes that might be originating from the PT-IFG and are reflected in post-stimulus alpha power reduction. These might foster distractor resistance by selecting and protecting memorandum representations from the distractor representations within visual cortical areas retaining the most selective mnemonic code.

Declaration of Competing Interest

The authors declare no competing interests.

Credit authorship contribution statement

Petra Hermann: Methodology, Software, Validation, Formal analysis, Investigation, Data curation, Writing – original draft, Writing – review & editing, Visualization. **Béla Weiss:** Methodology, Software, Validation, Formal analysis, Data curation, Writing – original draft, Writing – review & editing, Visualization. **Balázs Knakker:** Methodology, Software, Validation, Formal analysis, Investigation, Writing – original draft. **Petra Madurka:** Methodology, Software, Validation, Formal analysis, Investigation, Writing – original draft. **Annamária Manga:** Methodology, Software, Validation, Formal analysis, Investigation, Writing – original draft, Writing – review & editing. **Ádám Nárai:** Methodology, Software, Validation, Formal analysis, Writing – original draft, Writing – review & editing, Visualization. **Zoltán Vidnyánszky:** Conceptualization, Methodology, Formal analysis, Writing – original draft, Writing – review & editing, Supervision, Project administration, Funding acquisition.

Acknowledgement

This work was supported by grants from the Hungarian Brain Research Program (Nemzeti Agykutatási Program 2017–1.2.1-NKP-2017–00002) and the Hungarian Scientific Research Fund (K112093) to Zoltán Vidnyánszky.

Data and Code Availability Statement

Data supporting the findings of this study and the computer codes used for the data analyses are available from the corresponding author upon written request.

Supplementary materials

Supplementary material associated with this article can be found, in the online version, at doi:10.1016/j.neuroimage.2021.118650.

References

Allen, M., Poggiali, D., Whitaker, K., Marshall, T.R., Kievit, R.A., 2019. Raincloud plots: a multi-platform tool for robust data visualization. Wellcome Open Res. 4. doi:10.12688/wellcomeopenres.15191.1.

Awh, E., Jonides, J., 2001. Overlapping mechanisms of attention and spatial working memory. Trends Cogn. Sci. (Regul. Ed.) 5, 119–126. doi:10.1016/S1364-6613(00)01593-X.

Bacigalupo, F., Luck, S.J., 2019. Lateralized Suppression of Alpha-Band EEG Activity As a Mechanism of Target Processing. J. Neurosci. 39, 900–917. doi:10.1523/JNEUROSCI.0183-18.2018.

Bae, G.-Y., Luck, S.J., 2017. Interactions between visual working memory representations. Atten Percept Psychophys 79, 2376–2395. doi:10.3758/s13414-017-1404-8.

Bankó, É.M., Gál, V., Körtvélyes, J., Kovács, G., Vidnyánszky, Z., 2011. Dissociating the Effect of Noise on Sensory Processing and Overall Decision Difficulty. J. Neurosci. 31, 2663–2674. doi:10.1523/JNEUROSCI.2725-10.2011.

Bell, A.J., Sejnowski, T.J., 1995. An Information-Maximization Approach to Blind Separation and Blind Deconvolution. Neural Comput. 7, 1129–1159. doi:10.1162/neco.1995.7.6.1129.

Brainard, D.H., 1997. The Psychophysics Toolbox. Spat. Vis. 10, 433–436. doi:10.1163/156856897X00357.

Broadbent, D.E., Broadbent, M.H.P., 1981. Recency effects in visual memory. The Q. J. Experimental Psychol. Section A 33, 1–15. doi:10.1080/14640748108400762.

Cauley, S.F., Polimeni, J.R., Bhat, H., Wald, L.L., Setsompop, K., 2014. Interslice leakage artifact reduction technique for simultaneous multislice acquisitions. Magn. Reson. Med. 72, 93–102. doi:10.1002/mrm.24898.

Chaumon, M., Bishop, D.V.M., Busch, N.A., 2015. A practical guide to the selection of independent components of the electroencephalogram for artifact correction. J. Neurosci. Methods, Cutting-edge EEG Methods 250, 47–63. doi:10.1016/j.jneumeth.2015.02.025.

Chelazzi, L., Marini, F., Pascucci, D., Turatto, M., 2019. Getting rid of visual distractors: the why, when, how, and where. Current Opinion in Psychology. Attention & Perception 29, 135–147. doi:10.1016/j.copsyc.2019.02.004.

Chun, M.M., Golomb, J.D., Turk-Browne, N.B., 2011. A taxonomy of external and internal attention. Annu. Rev. Psychol. 62, 73–101. doi:10.1146/annurev.psych.093008.100427.

Clapp, W.C., Rubens, M.T., Gazzaley, A., 2010. Mechanisms of working memory disruption by external interference. Cereb. Cortex 20, 859–872. doi:10.1093/cercor/bhp150.

Conner, C.R., Ellmore, T.M., Pieters, T.A., DiSano, M.A., Tandon, N., 2011. Variability of the relationship between electrophysiology and BOLD-fMRI across cortical regions in humans. J. Neurosci. 31, 12855–12865. doi:10.1523/JNEUROSCI.1457-11.2011.

Courtney, S.M., Petit, L., Maisog, J.M., Ungerleider, L.G., Haxby, J.V., 1998. An area specialized for spatial working memory in human frontal cortex. ScienceScience 279, 1347–1351. doi:10.1126/science.279.5355.1347.

Courtney, S.M., Ungerleider, L.G., Keil, K., Haxby, J.V., 1997. Transient and sustained activity in a distributed neural system for human working memory. NatureNature 386, 608–611. doi:10.1038/386608a0.

de Vries, I.E.J., Slagter, H.A., Olivers, C.N.L., 2020. Oscillatory control over representational states in working memory. Trends Cogn. Sci. (Regul. Ed.) 24, 150–162. doi:10.1016/j.tics.2019.11.006.

Delorme, A., Makeig, S., 2004. EEGLAB: an open source toolbox for analysis of single-trial EEG dynamics including independent component analysis. J. Neurosci. Methods 134, 9–21. doi:10.1016/j.jneumeth.2003.10.009.

Delorme, A., Sejnowski, T., Makeig, S., 2007. Enhanced detection of artifacts in EEG data using higher-order statistics and independent component analysis. NeuroimageNeuroimage 34, 1443–1449. doi:10.1016/j.neuroimage.2006.11.004.

Desimone, R., Duncan, J., 1995. Neural mechanisms of selective visual attention. Annu. Rev. Neurosci. 18, 193–222. doi:10.1146/annurev.ne.18.030195.001205.

D'Esposito, M., Aguirre, G.K., Zarahn, E., Ballard, D., Shin, R.K., Lease, J., 1998. Functional MRI studies of spatial and nonspatial working memory. Cogn. Brain Res. 7, 1–13. doi:10.1016/S0926-6410(98)00004-4.

Dolcos, F., Miller, B., Kragel, P., Jha, A., McCarthy, G., 2007. Regional brain differences in the effect of distraction during the delay interval of a working memory task. Brain Res. 1152, 171–181. doi:10.1016/j.brainres.2007.03.059.

Donoghue, T., Haller, M., Peterson, E.J., Varma, P., Sebastian, P., Gao, R., Noto, T., Lara, A.H., Wallis, J.D., Knight, R.T., Shestyuk, A., Voytek, B., 2020. Parameterizing neural power spectra into periodic and aperiodic components. Nat. Neurosci. 23, 1655–1665. doi:10.1038/s41593-020-00744-x.

Downing, P.E., Jiang, Y., Shuman, M., Kanwisher, N., 2001. A Cortical Area Selective for Visual Processing of the Human Body. ScienceScience 293, 2470–2473. doi:10.1126/science.1063414.

Duchaine, B., Yovel, G., 2015. A Revised Neural Framework for Face Processing. Annu. Rev. Vis. Sci. 1, 393–416. doi:10.1146/annurev-vision-082114-035518.

Egner, T., Hirsch, J., 2005. Cognitive control mechanisms resolve conflict through cortical amplification of task-relevant information. Nat. Neurosci. 8, 1784–1790. doi:10.1038/nn1594.

Feredoes, E., Heinen, K., Weiskopf, N., Ruff, C., Driver, J., 2011. Causal evidence for frontal involvement in memory target maintenance by posterior brain areas during distracter interference of visual working memory. PNAS 108, 17510–17515. doi:10.1073/pnas.1106439108.

Freiwald, W., Duchaine, B., Yovel, G., 2016. Face Processing Systems: from Neurons to Real-World Social Perception. Annu. Rev. Neurosci. 39, 325–346. doi:10.1146/annurev-neuro-070815-013934.

Gao, R., Peterson, E.J., Voytek, B., 2017. Inferring synaptic excitation/inhibition balance from field potentials. NeuroimageNeuroimage 158, 70–78. doi:10.1016/j.neuroimage.2017.06.078.

Gayet, S., Guggenmos, M., Christophel, T.B., Haynes, J.-D., Paffen, C.L.E., der Stigchel, S.V., Sterzer, P., 2017. Visual Working Memory Enhances the Neural Response to Matching Visual Input. J. Neurosci. 37, 6638–6647. doi:10.1523/JNEUROSCI.3418-16.2017.

Gazzaley, A., 2011. Influence of early attentional modulation on working memory. Neuropsychologia, Attention and Short-Term Memory 49, 1410–1424. doi:10.1016/j.neuropsychologia.2010.12.022.

Gazzaley, A., Cooney, J.W., Rissman, J., D'Esposito, M., 2005. Top-down suppression deficit underlies working memory impairment in normal aging. Nat. Neurosci. 8, 1298–1300. doi:10.1038/nn1543.

Gazzaley, A., Nobre, A.C., 2012. Top-down modulation: bridging selective attention and working memory. Trends Cogn. Sci. (Regul. Ed.) 16, 129–135. doi:10.1016/j.tics.2011.11.014.

Girshick, A.R., Landy, M.S., Simoncelli, E.P., 2011. Cardinal rules: visual orientation perception reflects knowledge of environmental statistics. Nat. Neurosci. 14, 926–932. doi:10.1038/nn.2831.

Gorgoraptis, N., Catalao, R.F.G., Bays, P.M., Husain, M., 2011. Dynamic Updating of Working Memory Resources for Visual Objects. J. Neurosci. 31, 8502–8511. doi:10.1523/JNEUROSCI.0208-11.2011.

Gramfort, A., Luessi, M., Larson, E., Engemann, D.A., Strohmeier, D., Brodbeck, C., Goj, R., Jas, M., Brooks, T., Parkkonen, L., Hämäläinen, M., 2013. MEG and EEG data analysis with MNE-Python. Front. Neurosci. 7. doi:10.3389/fnins.2013.00267.

Griffin, I.C., Nobre, A.C., 2003. Orienting Attention to Locations in Internal Representations. J. Cogn. Neurosci. 15, 1176–1194. doi:10.1162/089892903322598139.

Griffiths, B.J., Mayhew, S.D., Mullinger, K.J., Jorge, J., Charest, I., Wimber, M., Hanslmayr, S., 2019. Alpha/beta power decreases track the fidelity of stimulus-specific information. eLife 8, e49562. https://doi.org/10.7554/eLife.49562

Grill-Spector, K., Kourtzi, Z., Kanwisher, N., 2001. The lateral occipital complex and its role in object recognition. Vision Res. 41, 1409–1422.

Grill-Spector, K., Weiner, K.S., Kay, K., Gomez, J., 2017. The Functional Neuroanatomy of Human Face Perception. Annu. Rev. Vis. Sci. 3, 167–196. doi:10.1146/annurev-vision-102016-061214.

Hayden, B.Y., Gallant, J.L., 2009. Combined effects of spatial and feature-based attention on responses of V4 neurons. Vision Res., Visual Attention: Psychophys., electrophysiol. neuroimaging 49, 1182–1187. doi:10.1016/j.visres.2008.06.011.

He, B.J., Zempel, J.M., Snyder, A.Z., Raichle, M.E., 2010. The Temporal Structures and Functional Significance of Scale-free Brain Activity. NeuronNeuron 66, 353–369. doi:10.1016/j.neuron.2010.04.020.

Hermes, D., Nguyen, M., Winawer, J., 2017. Neuronal synchrony and the relation between the blood-oxygen-level dependent response and the local field potential. PLoS Biol. 15, e2001461. doi:10.1371/journal.pbio.2001461.

Hillyard, S.A., Anllo-Vento, L., 1998. Event-related brain potentials in the study of visual selective attention. PNAS 95, 781–787. doi:10.1073/pnas.95.3.781.

Itthipuripat, S., Sprague, T.C., Serences, J.T., 2019. Functional MRI and EEG Index Complementary Attentional Modulations. J. Neurosci. 39, 6162–6179. doi:10.1523/JNEUROSCI.2519-18.2019.

Jha, A.P., Fabian, S.A., Aguirre, G.K., 2004. The role of prefrontal cortex in resolving distractor interference. Cognitive, Affective, & Behav. Neurosci. 4, 517–527. doi:10.3758/CABN.4.4.517.

Jonides, J., Nee, D.E., 2006. Brain mechanisms of proactive interference in working memory. NeuroscienceNeuroscience 139, 181–193. doi:10.1016/j.neuroscience.2005.06.042.

Kanwisher, N., McDermott, J., Chun, M.M., 1997. The fusiform face area: a module in human extrastriate cortex specialized for face perception. J. Neurosci. 17, 4302–4311.

Keil, A., Müller, M.M., 2010. Feature selection in the human brain: electrophysiological correlates of sensory enhancement and feature integration. Brain Res. 1313, 172–184. doi:10.1016/j.brainres.2009.12.006.

Kenemans, J.L., Kok, A., Smulders, F.T.Y., 1993. Event-related potentials to conjunctions of spatial frequency and orientation as a function of stimulus parameters and response requirements. Electroencephalography Clin. Neurophysiol./Evoked Potentials Section 88, 51–63. doi:10.1016/0168-5597(93)90028-N.

Kiyonaga, A., Egner, T., 2013. Working memory as internal attention: toward an integrative account of internal and external selection processes. Psychon. Bull. Rev. 20, 228–242. doi:10.3758/s13423-012-0359-y.

Kovács, G., Zimmer, M., Bankó, É., Harza, I., Antal, A., Vidnyánszky, Z., 2006. Electrophysiological Correlates of Visual Adaptation to Faces and Body Parts in Humans. Cereb. Cortex 16, 742–753. doi:10.1093/cercor/bhj020.

Landman, R., Spekreijse, H., Lamme, V.A.F., 2003. Large capacity storage of integrated objects before change blindness. Vision Res. 43, 149–164. doi:10.1016/S0042-6989(02)00402-9.

Lepsien, J., Nobre, A.C., 2007. Attentional Modulation of Object Representations in Working Memory. Cereb. Cortex 17, 2072–2083. doi:10.1093/cercor/bhl116.
Lopez-Calderon, J., Luck, S.J., 2014. ERPLAB: an open-source toolbox for the analysis of event-related potentials. Front. Hum. Neurosci. 8. doi:10.3389/fnhum.2014.00213.
Lorenc, E.S., Sreenivasan, K.K., Nee, D.E., Vandenbroucke, A.R.E., D'Esposito, M., 2018. Flexible Coding of Visual Working Memory Representations during Distraction. J. Neurosci. 38, 5267–5276. doi:10.1523/JNEUROSCI.3061-17.2018.
Manga, A., Vakli, P., Vidnyánszky, Z., 2020. The influence of anticipated monetary incentives on visual working memory performance in healthy younger and older adults. Sci. Rep. 10, 8817. doi:10.1038/s41598-020-65723-5.
Maris, E., Oostenveld, R., 2007. Nonparametric statistical testing of EEG- and MEG-data. J. Neurosci. Methods 164, 177–190. doi:10.1016/j.jneumeth.2007.03.024.
McCarthy, G., Puce, A., Gore, J.C., Allison, T., 1997. Face-specific processing in the human fusiform gyrus. J. Cogn. Neurosci. 9, 605–610. doi:10.1162/jocn.1997.9.5.605.
Myers, N.E., Rohenkohl, G., Wyart, V., Woolrich, M.W., Nobre, A.C., Stokes, M.G., 2015. Testing sensory evidence against mnemonic templates. Elife 4, e09000. doi:10.7554/eLife.09000.
Myers, N.E., Stokes, M.G., Nobre, A.C., 2017. Prioritizing Information during Working Memory: beyond Sustained Internal Attention. Trends Cogn. Sci. (Regul. Ed.) 21, 449–461. doi:10.1016/j.tics.2017.03.010.
Nee, D.E., Brown, J.W., Askren, M.K., Berman, M.G., Demiralp, E., Krawitz, A., Jonides, J., 2013. A Meta-analysis of Executive Components of Working Memory. Cereb. Cortex 23, 264–282. doi:10.1093/cercor/bhs007.
Nee, D.E., D'Esposito, M., 2018. Working Memory, in: stevens' Handbook of Experimental Psychology and Cognitive Neuroscience. Am. Cancer Society 1–26. doi:10.1002/9781119170174.epcn112.
Nee, D.E., Jonides, J., 2009. Common and distinct neural correlates of perceptual and memorial selection. NeuroimageNeuroimage 45, 963–975. doi:10.1016/j.neuroimage.2009.01.005.
Nee, D.E., Jonides, J., 2008. Neural correlates of access to short-term memory. PNAS 105, 14228–14233. doi:10.1073/pnas.0802081105.
Nelissen, N., Stokes, M., Nobre, A.C., Rushworth, M.F.S., 2013. Frontal and parietal cortical interactions with distributed visual representations during selective attention and action selection. J. Neurosci. 33, 16443–16458. doi:10.1523/JNEUROSCI.2625-13.2013.
Nichols, T.E., Holmes, A.P., 2002. Nonparametric permutation tests for functional neuroimaging: a primer with examples. Hum. Brain Mapp. 15, 1–25. doi:10.1002/hbm.1058.
Nobre, A.C., Stokes, M.G., 2019. Premembering Experience: a Hierarchy of Time-Scales for Proactive Attention. NeuronNeuron 104, 132–146. doi:10.1016/j.neuron.2019.08.030.
Noonan, M.P., Crittenden, B.M., Jensen, O., Stokes, M.G., 2018. Selective inhibition of distracting input. Behav. Brain Res. 355, 36–47. doi:10.1016/j.bbr.2017.10.010, SI: MCC 2016.
Olivers, C.N.L., Meijer, F., Theeuwes, J., 2006. Feature-based memory-driven attentional capture: visual working memory content affects visual attention. J. Exp. Psychol. Hum. Percept. Perform. 32, 1243–1265. doi:10.1037/0096-1523.32.5.1243.
Olivers, C.N.L., Peters, J., Houtkamp, R., Roelfsema, P.R., 2011. Different states in visual working memory: when it guides attention and when it does not. Trends Cogn. Sci. (Regul. Ed.) 15, 327–334. doi:10.1016/j.tics.2011.05.004.
Onton, J., Westerfield, M., Townsend, J., Makeig, S., 2006. Imaging human EEG dynamics using independent component analysis. Neurosci. Biobehav. Rev., Methodological and Conceptual Advances in the Study of Brain-Behavior Dynamics: A Multivariate Lifespan Perspective 30, 808–822. doi:10.1016/j.neubiorev.2006.06.007.
Oostenveld, R., Fries, P., Maris, E., Schoffelen, .J..-M., 2010. FieldTrip: open Source Software for Advanced Analysis of MEG, EEG, and Invasive Electrophysiological Data [WWW Document]. Computational Intelligence and Neuroscience. https://doi.org/10.1155/2011/156869
Pelli, D.G., 1997. The VideoToolbox software for visual psychophysics: transforming numbers into movies. Spat. Vis. 10, 437–442. doi:10.1163/156856897X00366.
Pernet, C.R., 2014. Misconceptions in the use of the General Linear Model applied to functional MRI: a tutorial for junior neuro-imagers. Front. Neurosci. 8. doi:10.3389/fnins.2014.00001.
Pernet, C.R., Wilcox, R.R., Rousselet, G.A., 2013. Robust Correlation Analyses: false Positive and Power Validation Using a New Open Source Matlab Toolbox. Front. Psychol. 3. doi:10.3389/fpsyg.2012.00606.
Pinsk, M.A., Arcaro, M., Weiner, K.S., Kalkus, J.F., Inati, S.J., Gross, C.G., Kastner, S., 2009. Neural representations of faces and body parts in macaque and human cortex: a comparative fMRI study. J. Neurophysiol. 101, 2581–2600. doi:10.1152/jn.91198.2008.
Pitcher, D., Walsh, V., Yovel, G., Duchaine, B., 2007. TMS evidence for the involvement of the right occipital face area in early face processing. Curr. Biol. 17, 1568–1573. doi:10.1016/j.cub.2007.07.063.
Podvalny, E., Noy, N., Harel, M., Bickel, S., Chechik, G., Schroeder, C.E., Mehta, A.D., Tsodyks, M., Malach, R., 2015. A unifying principle underlying the extracellular field potential spectral responses in the human cortex. J. Neurophysiol. 114, 505–519. doi:10.1152/jn.00943.2014.
Poldrack, R.A., Mumford, J.A., Nichols, T.E., 2011. Handbook of Functional MRI Data Analysis. Cambridge University Press, Cambridge doi:10.1017/CBO9780511895029.
Polich, J., 2007. Updating P300: an integrative theory of P3a and P3b. Clin. Neurophysiol. 118, 2128–2148. doi:10.1016/j.clinph.2007.04.019.
Previc, F.H., Harter, M.R., 1982. Electrophysiological and behavioral indicants of selective attention to multifeature gratings. Percept. Psychophys. 32, 465–472. doi:10.3758/BF03202777.
Rademaker, R.L., Chunharas, C., Serences, J.T., 2019. Coexisting representations of sensory and mnemonic information in human visual cortex. Nat. Neurosci. 22, 1336–1344. doi:10.1038/s41593-019-0428-x.
Rossion, B., Hanseeuw, B., Dricot, L., 2012. Defining face perception areas in the human brain: a large-scale factorial fMRI face localizer analysis. Brain Cogn. 79, 138–157. doi:10.1016/j.bandc.2012.01.001.
Sakai, K., Rowe, J.B., Passingham, R.E., 2002. Active maintenance in prefrontal area 46 creates distractor-resistant memory. Nat. Neurosci. 5, 479–484. doi:10.1038/nn846.
Scheeringa, R., Koopmans, P.J., Mourik, T.van, Jensen, O., Norris, D.G., 2016. The relationship between oscillatory EEG activity and the laminar-specific BOLD signal. PNAS 113, 6761–6766. doi:10.1073/pnas.1522577113.
Serences, J.T., 2016. Neural mechanisms of information storage in visual short-term memory. Vision Res. 128, 53–67. doi:10.1016/j.visres.2016.09.010.
Setsompop, K., Gagoski, B.A., Polimeni, J.R., Witzel, T., Wedeen, V.J., Wald, L.L., 2012. Blipped-Controlled Aliasing in Parallel Imaging (blipped-CAIPI) for simultaneous multi-slice EPI with reduced g-factor penalty. Magn. Reson. Med. 67, 1210–1224. doi:10.1002/mrm.23097.
Sligte, I.G., Scholte, H.S., Lamme, V.A.F., 2009. V4 Activity Predicts the Strength of Visual Short-Term Memory Representations. J. Neurosci. 29, 7432–7438. doi:10.1523/JNEUROSCI.0784-09.2009.
Smid, H.G.O.M., Jakob, A., Heinze, .H..-J., 1999. An event-related brain potential study of visual selective attention to conjunctions of color and shape. Psychophysiology 36, 264–279. doi:10.1017/S0048577299971135.
Soto, D., Hodsoll, J., Rotshtein, P., Humphreys, G.W., 2008. Automatic guidance of attention from working memory. Trends Cogn. Sci. (Regul. Ed.) 12, 342–348. doi:10.1016/j.tics.2008.05.007.
Souza, A.S., Oberauer, K., 2016. In search of the focus of attention in working memory: 13 years of the retro-cue effect. Atten. Percept. Psychophys. 78, 1839–1860. doi:10.3758/s13414-016-1108-5.
Sreenivasan, K.K., Jha, A.P., 2007. Selective Attention Supports Working Memory Maintenance by Modulating Perceptual Processing of Distractors. J Cogn Neurosci 19, 32–41. doi:10.1162/jocn.2007.19.1.32.
Stigliani, A., Jeska, B., Grill-Spector, K., 2019. Differential sustained and transient temporal processing across visual streams. PLoS Comput. Biol. 15, e1007011. doi:10.1371/journal.pcbi.1007011.
Sugase-Miyamoto, Y., Liu, Z., Wiener, M.C., Optican, L.M., Richmond, B.J., 2008. Short-Term Memory Trace in Rapidly Adapting Synapses of Inferior Temporal Cortex. PLoS Comput. Biol. 4, e1000073. doi:10.1371/journal.pcbi.1000073.
Van Diepen, R.M., Foxe, J.J., Mazaheri, A., 2019. The functional role of alpha-band activity in attentional processing: the current zeitgeist and future outlook. Curr. Opinion in Psychol., Attention & Perception 29, 229–238. doi:10.1016/j.copsyc.2019.03.015.
Van Diepen, R.M., Miller, L.M., Mazaheri, A., Geng, J.J., 2016. The role of alpha activity in spatial and feature-based attention. eNeuro 3. doi:10.1523/ENEURO.0204-16.2016.
van Ede, F., Chekroud, S.R., Stokes, M.G., Nobre, A.C., 2019. Concurrent visual and motor selection during visual working memory guided action. Nat. Neurosci. 22, 477–483. doi:10.1038/s41593-018-0335-6.
Vanni, S., Revonsuo, A., Hari, R., 1997. Modulation of the parieto-occipital alpha rhythm during object detection. J. Neurosci. 17, 7141–7147. doi:10.1523/JNEUROSCI.17-18-07141.1997.
Virtanen, P., Gommers, R., Oliphant, T.E., Haberland, M., Reddy, T., Cournapeau, D., Burovski, E., Peterson, P., Weckesser, W., Bright, J., van der Walt, S.J., Brett, M., Wilson, J., Millman, K.J., Mayorov, N., Nelson, A.R.J., Jones, E., Kern, R., Larson, E., Carey, C.J., Polat, İ., Feng, Y., Moore, E.W., VanderPlas, J., Laxalde, D., Perktold, J., Cimrman, R., Henriksen, I., Quintero, E.A., Harris, C.R., Archibald, A.M., Ribeiro, A.H., Pedregosa, F., van Mulbregt, P., 2020. SciPy 1.0: fundamental algorithms for scientific computing in Python. Nat. Methods 17, 261–272. doi:10.1038/s41592-019-0686-2.
Webster, M.A., MacLeod, D.I.A., 2011. Visual adaptation and face perception. Philosophical Trans. Royal Society B: Biological Sci. 366, 1702–1725. doi:10.1098/rstb.2010.0360.
Weiner, K.S., Grill-Spector, K., 2010. Sparsely-distributed organization of face and limb activations in human ventral temporal cortex. NeuroimageNeuroimage 52, 1559–1573. doi:10.1016/j.neuroimage.2010.04.262.
Weiner, K.S., Sayres, R., Vinberg, J., Grill-Spector, K., 2010. fMRI-adaptation and category selectivity in human ventral temporal cortex: regional differences across time scales. J. Neurophysiol. 103, 3349–3365. doi:10.1152/jn.01108.2009.
Wu, J., Ngo, G.H., Greve, D., Li, J., He, T., Fischl, B., Eickhoff, S.B., Yeo, B.T.T., 2018. Accurate nonlinear mapping between MNI volumetric and FreeSurfer surface coordinate systems. Hum. Brain Mapp. 39, 3793–3808. doi:10.1002/hbm.24213.
Yoon, J.H., Curtis, C.E., D'Esposito, M., 2006. Differential effects of distraction during working memory on delay-period activity in the prefrontal cortex and the visual association cortex. NeuroimageNeuroimage 29, 1117–1126. doi:10.1016/j.neuroimage.2005.08.024.
Yovel, G., 2016. Neural and cognitive face-selective markers: an integrative review. Neuropsychologia, Special Issue: Functional Selectivity in Perceptual and Cogn. Sys. - A Tribute to Shlomo Bentin (1946-2012) 83, 5–13. doi:10.1016/j.neuropsychologia.2015.09.026.
Zhen, Z., Yang, Z., Huang, L., Kong, X., Wang, X., Dang, X., Huang, Y., Song, Y., Liu, J., 2015. Quantifying interindividual variability and asymmetry of face-selective regions: a probabilistic functional atlas. NeuroimageNeuroimage 113, 13–25. doi:10.1016/j.neuroimage.2015.03.010.
Zumer, J.M., Scheeringa, R., Schoffelen, J.-.M., Norris, D.G., Jensen, O., 2014. Occipital alpha activity during stimulus processing gates the information flow to object-selective cortex. PLoS Biol. 12, e1001965. doi:10.1371/journal.pbio.1001965.